RXTE AND CHANDRA OBSERVATIONS OF GALACTIC MICROQUASARS GRO J1655-40 AND GRS 1915+105

A THESIS SUBMITTED TO
THE GRADUATE SCHOOL OF NATURAL AND APPLIED SCIENCES
OF
MIDDLE EAST TECHNICAL UNIVERSITY

BY

GÜL ESRA BÜLBÜL

IN PARTIAL FULFILLMENT OF THE REQUIREMENTS
FOR
THE DEGREE OF MASTER OF SCIENCE
IN
PHYSICS

JULY 2006

Approval of the Graduate School of Natural and Applied Sciences.

Prof. Dr. Canan Özgen
Director

I certify that this thesis satisfies all the requirements as a thesis for the degree of Master of Science.

Prof. Dr. Sinan Bilikmen
Head of Department

This is to certify that we have read this thesis and that in our opinion it is fully adequate, in scope and quality, as a thesis for the degree of Master of Science.

Assist. Prof. Dr. Sıtkı Çağdaş İnam
Co-Supervisor

Prof. Dr. Altan Baykal
Supervisor

Examining Committee Members

Prof. Dr. Ümit Kızıloğlu (METU, PHYS) _____

Prof. Dr. Altan Baykal (METU, PHYS) _____

Assist. Prof. Dr. S. Çağdaş İnam (BAŞKENT U, E.E.) _____

Assist. Prof. Dr. Ersin Göğüş (SABANCI U, N.S.E.) _____

Assist. Prof. Dr. S. Kaan Yerli (METU, PHYS) _____

I hereby declare that all information in this document has been obtained and presented in accordance with academic rules and ethical conduct. I also declare that, as required by these rules and conduct, I have fully cited and referenced all material and results that are not original to this work.

Name, Lastname: Gül Esra Bülbül

Signature :

ABSTRACT

RXTE AND CHANDRA OBSERVATIONS OF GALACTIC MICROQUASARS GRO J1655-40 AND GRS 1915+105

BÜLBÜL, GÜL ESRA

M.S., Department of Physics

Supervisor: Prof. Dr. Altan Baykal

Co-Supervisor: Assist. Prof. Dr. Sıtkı Çağdaş İnam

July 2006, 87 pages.

In this thesis, RXTE timing analysis of Galactic Microquasars GRO J1655-40 and GRS 1915+105, the Chandra and RXTE joint spectral analysis of GRS 1915+105 are presented. We have investigated quasi periodic oscillations (QPOs) in the black hole binaries GRO J1655-40 and GRS 1915+105 observed in 99 and 122 observations made by the Proportional Counter Array (PCA) on board Rossi X-Ray Timing Explorer (RXTE) in both low energy band (2-12 keV) and high energy band (13-27 keV), respectively. Four different X-ray states are seen in the combined characteristics of power spectra, light curves extracted by using All Sky Monitor (ASM) and spectra during 1996 and 2005. Timing analysis of RXTE observations of both of two black hole binaries GRO J1655-40 and GRS 1915+105 displays twin high frequency quasi periodic oscillations (QPOs) which are sometimes simultaneous in high energy band. It is also shown that the time averaged 30 ksec Chandra grating spectrum analysis and RXTE spectrum analysis of recent observation of GRS 1915+105 in the very high state are consistent with the parameters which were mentioned before. We briefly discussed our results and the models on black hole spin and mass.

Keywords: Galactic Microquasars, GRO J1655-40, GRS 1915+105, RXTE and Chandra simultaneous spectral analysis, quasi periodic oscillations (QPOs)

ÖZ

GALAKTİK MİKROKUAZARLAR GRO J1655-40 VE GRS 1915+105 İN CHANDRA VE RXTE GÖZLEMLERİ

BÜLBÜL, GÜL ESRA

Yüksek Lisans , Fizik Bölümü

Tez Yöneticisi: Prof. Dr. Altan Baykal

Ortak Tez Yöneticisi: Assist. Prof. Dr. Sıtkı Çağdaş İnam

Temmuz 2006, 87 sayfa.

Bu tezde Galaktik mikrokuazarlar GRO J1655-40 ve GRS 1915+105 RXTE zamanlı gözlem analizleri, Chandra ve RXTE eş anlı gözlem analizleri sunulmaktadır. GRO J1655-40 in 99 Rossi X-ışınımı zamanlı teleskopu ile yapılmış 99 gözleminde ve GRS 1915+105 in Rossi X-ışınımı zamanlama teleskopuyla ile yapılmış 122 gözleminde yüksek frekans periyodiğimsi salınımları hem yüksek enerji bandında (13-27 keV) hemde düşük enerji (2-12 keV) bandında aradık. Bu kaynakların güç tayflarında ve ışık eğrilerinde 4 X-ışını durumu görülmüştür. RXTE zamanlama analizleri ikiz periyodiğimsi salınımları gösterir ve bu salınımlar yüksek enerji bandında zaman zaman aynı anda görülür. 30 ks Chandra ve RXTE eş anlı gözlemlerinin tayflarındaki güç yasası ve disk kara cisim parametrelerinin daha önceden yayınlanmış makalelerdeki parametrelerle tutarlı olduğu görülmüştür. Bulduğumuz sonuçların ve modellerin karadelik kütlesine ve dönmesine etkisini kısaca tartıştık.

Anahtar Sözcükler: Galaktik Mikrokuazarlar, GRO J1655-40, GRS 1915+105, RXTE ve Chandra ortak tayfları, periyodiğimsi salınımlar.

To My Mother

ACKNOWLEDGMENTS

I would like to express my deepest gratitude to my supervisor, Prof. Dr. Altan Baykal for his guidance and insight throughout the research. His insight has been of great help in overcoming many of the difficulties which arose throughout my master program. I would like to send my sincere gratefulness to my co-supervisor Assist. Prof. Dr. Sıtkı Çağdaş İnam for his great effort, guidance and support during this study.

I would like to thank Dr. Ersin Göğüş for many helpful discussions and suggestions on Chandra analysis and valuable helps on my academic career.

My special thank goes to Elif Beklen and Sibel Ersan for helpful discussions and encouragement during this study. Special thanks are due to Assist. Prof. Dr. Sinan Kaan Yerli and Dr. Seçil Gergün for extending timely help in carrying out some important Latex works.

I especially thank my mother and dear sister for their endless love and care all through my life.

My greatest attitude goes to Beste Korutlu for their endless understanding, her constant friendly support and an extraordinary source of advice.

Last but not least, my deepest thanks go to Mustafa Huş who gave me exact right motivation and valuable support I needed in order to continue.

TABLE OF CONTENTS

LIST OF TABLES

LIST OF FIGURES

CHAPTER 1

OVERVIEW

A microquasar is an X-ray binary system consisting of an accreting companion star and a stellar mass black hole. The black hole exhibits jets of highly relativistic particles ejected away perpendicular to the accretion disk. Ejected particle outflow produces synchrotron emission which is detectable in radio and infrared band of the energy spectrum. The matter accreted from the companion star to the black hole is responsible for the X- ray signature.

Since similar accretion mechanism and jet formation system have been seen in quasars which also consist of a compact object, namely a black hole, stellar mass black holes X-ray binaries are called microquasars. But in quasars, the black hole is supermassive (millions of solar masses); in microquasars, the black hole mass is a few solar masses. From the observations of two sided moving jets, it was inferred that ejecta in microquasars move with relativistic speeds similar to those believed to be present in quasars (Mirabel & Rodrigues, 1999). The galactic microquasar GRO J1655-40 was discovered in outburst at a level of 2.2 $\times 10^8$ ergs cm^{-2} s^{-1} in 20-200 keV energy band on July 27, 1994 with the Burst and Transient Source Experiment (BATSE) on board Compton Gamma Ray Observatory (CGRO). During its 1994 outburst radio-loud superluminal jets were observed (Tingay

et al 1995, Hjellming & Ruben 1995). Rossi X-ray Timing Explorer (RXTE) detected X-ray variability in late 1996 outburst of GRO J1655-40 which lasted about 6 days (Remillard et al, 1996). GRO J1655-40 showed high frequency quasi-periodic oscillations (QPOs) (100-450 Hz) which have been observed with RXTE. GRS 1915+105 is a galactic microquasar which was discovered by GRANAT/ WATCH (Castro-Tirado 1994). It has showed series of outbursts since it has been discovered. GRS 1915+105 displays high frequency quasi-periodic oscillations (QPOs) 40 Hz and 67 Hz which were observed with RXTE.

In this thesis we present high frequency X-ray QPO signature of both microquasars GRO J1655-40 and GRS 1915+105 using Rossi X-ray Timing Explorer (RXTE) Proportional Counter Array (PCA) data. We expect to observe four previously discovered high frequency QPOs peaking at ~ 450 Hz in high energy band ($\sim 13 - 27$ keV) and at ~ 300 Hz in low energy band ($\sim 2 - 12$ keV) (Remillard et al 1999b, Strohmayer, 2001) in 1996-1997 and 2004-2005 outbursts observations of GRO J1655-40 and both ~ 40 Hz and ~ 67 Hz QPOs which were detected in the same observations in 1996-1997 and 2004-2005 observations of black hole binary GRS 1915+105 (Morgan et al. 1997, Strohmayer 2001b).

In this thesis, we use the data sets from observations of galactic microquasars GRO J1655-40 and GRS 1915+105 1 with RXTE (Rossi X-ray Timing Explorer) and Chandra X-ray Observatory. The next chapter consists of the fundamental observational properties blackhole binaries. In Chapters 3 and 4, analysis of RXTE observations of GRO J1655-40 and GRS 1915+105 is presented respectively. Chapter 5 is about spectral results of our analysis of RXTE and Chandra

observations of GRS 1915+105. In conclusion we discussed briefly the implication of our observational results on black hole mass limits and black hole spin.

CHAPTER 2

INTRODUCTION

Since 1972, the data obtained in hard X-ray and gamma ray band of the electromagnetic spectrum with CGRO (Compton Gamma Ray Observatory), Beppo-SAX, GRANAT, INTEGRAL (The International Gamma-Ray Astrophysics Laboratory) and in X-ray band with Chandra (Chandra X-ray Observatory), RXTE (Rossi X-ray Timing Explorer), XMM-Newton (X-ray Multi-Mirror Mission), ROSAT (The Roentgen Satellite), GINGA (Japanese for 'galaxy'), ASCA (The Advanced Satellite for Cosmology and Astrophysics)have been used to find about 250 X-ray binaries 15 % of which are microquasars in our galaxy. From now on ASTRO E-2 will serve us to examine the new sources in the X-ray band of the electromagnetic spectrum. With the capability of monitoring other satellites, the outbursts of X-ray transients and emergence of high states of persistent sources have been examined in other wavelengths. This is the reason why we have wealth of information on X-ray binaries.

Webster & Murdin (1972) and Bultin (1972) discovered the first black hole binary (BHB) Cyg X-1 followed by the discovery of LMC X-3 (Cowley et al. 1983). There are 18 confirmed black hole binaries and 22 black hole candidates in our galaxy (McClintock & Remillard, 2004). Recent studies about black hole

binaries have been extensively reviewed (McClintock & Remillard, 2004).

X-ray binaries (XRB) consist of a compact object (white dwarf, neutron star, black hole) and a companion star which accretes mass onto the compact object. XRBs are classified as high-mass X-ray binaries (HMXB) and low-mass X-ray binaries (LMXB) depending on the mass of the companion star.

High-mass X-ray binaries consist of population I stars of O-B spectral type, concentrated at the spiral arms of the galaxy, are orbited by a compact X-ray source; a neutron star, a black hole or a white dwarf. HMXBs are divided into two groups; those in which the primary is a Be star (Be/X-ray binary) and those in which the primary is a supergiant (SG/X-ray binary).

i- SG/X-ray binary's companion star is a supergiant whose spectral type is earlier than B2 or Of stars. The companions are very massive ($\sim$ 18 to over 40 $M_{\odot}$), some of them contain black hole (Cyg X-1). Their orbital periods are generally less than $\sim$ 10 days. Most of the SG/X-ray binaries are persistent X-ray sources. The companion star fills its Roche lobe, and the accretion flow is dense enough to power a strong X-ray source (LMC X-3, LMC X-4, Cen X-3).

ii- The Be or Oe stars are the companions which are of lower mass ($\sim$ 8 to about 20 $M_{\odot}$) of the Be/X-ray binaries. About 80 % of them are transients (for a catalogue of HMXBs see Lui et al. 2000). Their orbital periods are generally longer compared to the SG/X-ray binaries ($>$ 20 days). The main mass transfer mechanism of these OB giants is accretion via stellar

wind. The stellar wind is strong enough in massive stars to capture material from the companion star (Vela X-1, A0620). Roche-lobe overflow is also important mass transfer mechanism in Be type X-ray binaries (Van Paradijs 1983).

Low-mass X-ray binaries (LMXBs) consist of a late type or degenerate low mass ($< 2.5 M_{\odot}$) donor star with spectral type K and M. Since the donor star is an old star, LMXBs are located near the galactic bulge. The mass transfer occurs via Roche-lobe overflow. The low mass companion star fills its Roche Lobe and begins to accrete mass having large angular momentum onto the collapsed star. The orbital periods of the LMXBs are relatively short ranging from ~ 0.19 hour to ~ 398 hours.

LMXBs fall into two groups; persistent or transient X-ray sources. Persistent LMXBs (GX 339-4) are detected easily and visible most of the times since their X-ray luminosities are $\sim 10^{37}$ ergs s^{-1}. Sco X-1, Cyg X-2 are typical examples of the persistent LMXBs (Stella et al. 1999). Transient LMXBs (A0620-00) are faint. They spend most of their time in quiescence state ($L_x < 10^{30}$ergs s^{-1}). During sudden few month long X-ray outbursts their luminosities reach up to $10^{36} - 10^{38}$ergs s^{-1} (Van Paradijs 1995).

2.1 MICROQUASARS

Microquasars are the X-ray binaries composed of a stellar mass black hole and an accreting companion. The binary system transfers matter from companion to

the black hole and the matter spiraling around the black hole is the source of emitting X-rays. They also produce jets which are the source of powerful radio emission (Mirabel & Rodriguez 1999).

The radiation of black hole binaries is dominated by X-ray component which radiates from inner accretion disk. The five canonical X-ray spectral states have been identified in XRBs; very high state (VHS), high-soft state (HS), intermediate state (IS), low-hard state (LS) and quiescence state (QS) based upon their strength of their X-ray emission (Van Der Klis 1995). These states differ by luminosity, the power-law photon index, spectral and timing behavior of X-rays.

2.1.1 Quiescence State(QS)

XRBs stay almost 99 % of their time in their quiescence state. The matter transfer rate from the companion is very low, the luminosity is below 10^{33} ergs s^{-1} (Mirabel & Rodriguez 1999).

The spectrum is hard and non-thermal. Long period systems and short period systems differ by their luminosity in their quiescence state. The long period systems are brighter in their QS, because the nuclear evolution of the companion governs the mass transfer mechanism rather than gravitational radiation (Menou et al. 1999). V404 Cyg is a long period X-ray binary which has 155.3 hr orbital period and its luminosity is about 10^{33} ergs s^{-1} (Kong et al. 2002). The short period systems have low luminosity in their quiescence state. A0620-00 is a X-ray nova having orbital period 7.8 hr and luminosity 10^{30} ergs s^{-1} (McClintock et al. 1995; Narayan et al. 1996).

The radio emission is weak during quiescence state. This is supported by GX 339-4 when it is in quiescence (Corbel et al. 2003).

Advection Dominated Accretion Disk (ADAF/disk) model accounts well for the observed properties of black hole binaries in their quiescence state.

i- The power law spectrum is hard (Narayan et al. 1996; Narayan et al. 1997; Hameury et al.1997; Quataert & Narayan 1999; McClintock et al. 2003).

ii- Black hole binaries are faint relative to neutron star binaries (Narayan et al. 2002).

iii- Several day retardation in optical/UV light curve when X-ray novae go into burst (Hameury et al. 1997)

iv- Broad band spectrum is usually seen (McClintock et al. 2003)

v- The disk is truncated (see Figure 2.1) (Narayan 1996; Esin et al. 1997; McClintock et al. 2001b; McClintock et al. 2003a).

During the quiescence state, the accretion rate is very low. As a result of a thermal instability and rapid increase in the accretion rate, the outburst is initiated. The hard X-rays grow first then the soft X-ray produces, the system enters its very high state, and the high-soft state tends to evolve into the intermediate state and low-hard state before entering again its quiescence phase. But this pattern is not applicable to all black hole binaries. GRO J0422+32 and GRS 1716-249 have been observed only in their low-hard state (Goldwurm 2002).

2.1.2 The Radio Quite High-Soft State(HS)

At luminosities (0.01-0.2) L_{edd}, the X-ray spectra of XRBs soften and the thermal component dominates the spectrum (Remillard 2001). The soft X-ray component represents thermal emission from the disk. Steeply falling power law component associated with inverse Compton scattering is also present (Γ =2.1-4.8) (McClintock & Remillard 2004). The high-soft phase spectra have been modeled by multi-color accretion disk model (MCD). Multi-color disk model is based on standard disk model where the advection energy is negligible and the gravitational and irradiative transfer to the thermal radiation is considerable in Keplerian motion. The disk is optically thick and geometrically thin in this model. The key feature of MCD model is temperature of the inner disk $kT_i \approx 10eV$ for active galactic nuclei (AGN) $kT \approx 1keV$ for black hole binaries (BHB) (Shakura & Sunyaev 1973; Mitsuda et al. 1984).

The radio outflow is sharply quenched so the jet formation is suppressed by factor ≥ 25 (Tananbaum et al. 1972; Fender at al. 1999a; Gallo, Fender & Pooley 2003).

The thermal dominant state power density spectrum generally shows no QPOs. But a 0.3 % rms QPO at 27 Hz in 27 observations (1997 soft state) of GRO J1655-40 (Remillard 1999b) and 17 Hz 0.3 % QPO in 69 observations of XTE 1550-564 in soft state during 1998-1999 outburst were seen (Homan et al. 2001).

2.1.3 Low-Hard State (LS)

At lower luminosities $L_x < 0.01 L_{edd}$ spectrum is dominated by hard power law that extends to $\geq$ 100keV with exponential cut off ($1.5 < \Gamma < 2.1$) (Nowak 1995; Poutanen 1999; Remillard 2005).

The low-hard state (LS) spectrum is explained with ADAF/disk model (Esin et al. 2001) and synchrotron model (Markoff et al. 2001). In this model the material transferred from companion star initially forms an optically thick, cool disk (Shakura & Sunyaev 1973) outside the radius $30R_{sh} < R_{tr} < 100R_{sh}$. Inside this radius, the gas accretes via an optically thin, hot advection-dominated accretion. At this stage $10^{-2} < \dot{m} < 10^{-1}$ the luminosity is higher than that of the quiescent state (for a review see Narayan, Quartaert & Mahadevan 1998).

The comptonization becomes important in this stage. The hard X-ray component arises via inverse comptonization which is the seeding of photons by the high energy electrons. The LS of soft X-ray transient XTE J1118+480 is explained with ADAF/disk model (Esin et al. 2001), synchrotron model (Markoff et al. 2001) and thermal comptonization model (Frontera et al. 2001b).

The low-hard state is radio active. The X-ray emission is associated with persistent radio emission with flat spectrum. The steady self absorbed non-thermal jet is subject to the strong radio and infrared, optical band emission. Sco X-1 was the first X-ray binary which shows such radio behavior (Ables 1969; Wade & Hjellming 1971; Hjellming & Johnston 1988).

Broad QPOs, sometimes referred as peak noise are seen at low frequency in

low-hard state. These oscillations can attain amplitudes as high as 30-40 % of the average flux at 1-5 Hz (Morgan, Remillard & Greiner 1997; Cui et al. 1999). The QPOs frequency at the beginning of the low-hard state of GRS 1915+105 was 2.3 Hz, decrease slowly to a lowest frequency of 0.62 Hz and again increased slowly to 2.0 Hz towards the end of the LS (Paul et al. 1998).

2.1.4 Very High State (VHS)

The very high state redefined as Steep Power-Law State (SPL) occurs when the luminosity of BHB is high ($L_x > 0.2L_{edd}$). The photon index is ($\Gamma \geq 2.4$)

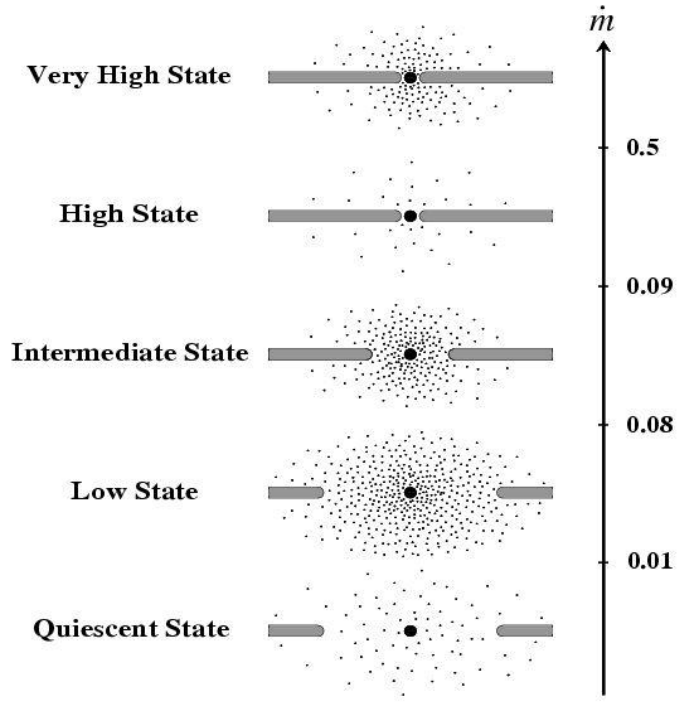

Figure 2.1: Schematic view of accretion in X-ray States as a function of the total Eddingtonscaled mass accretion rate $\dot{m}$. The ADAF is represented by dots and the thin disk by the horizontal bars. The very high state is illustrated, but it is not included in the unification scheme (Esin et al. 1997).

steeper than that of the low hard state ($\Gamma \approx 1.7$). The non-thermal power density spectrum generally shows quasi-periodic oscillations (QPOs) in the range of 0.1-30 Hz (McClintock & Remillard 2004). The X-ray QPOs first detected with GINGA in GX 339-4 (Miyamoto & Kitamoto 1991) and GRS 1124-683 (Miyamoto et al. 1993) during their bright outbursts.

CGRO observations exhibit very high state extends to photon energies up to 800keV (Remillard 2005). Hard state spectra show cut-off near 100 keV (Grove et al. 1998) but there is no evidence for the high energy cut-off for VHS spectra. Although the unbroken power-law spectra which are accompanied by the presence of X-ray QPOs were observed by OSSE for five BHBs in very high state (McClintock & Remillard 2004), RXTE observations show that some sources exhibit both X-ray high frequency QPOs at 100-450 Hz and steep power law spectrum (Remillard et al. 2002b). This is why McClintock & Remillard (2004) redefined the very high state as steep power law state (SPL).

The origin of the steep power law component is interpreted as the result of the inverse Compton scattering. But the important thing is that the high frequency QPOs 100-450 Hz in seven BHB is associated with the SPL spectrum (McClintock & Remillard 2004). Generally accretion disk becomes visible in X-ray spectrum of the SPL state. The inverse Compton scattering is also important mechanism to seed photons (Zdziarski 2000). Most of the models suggest that the MeV photons produced in the non-thermal corona via comptonization by seed photons of keV photons (Gierlinski et al. 1999). The disk appears as hot and small. This is the effect of radiative transfer mechanisms that occurs when the disk is viewed

through a compact corona with moderate optical depth (Kubota & Makishima 2004).

SPL state is associated with the discrete and powerful jets which have the Lorentz factor ($\tau > 2$) (Fender & Maccarone 2003) although GRO J1655-40 and XTE J1550-564 shows different behavior. During the 1996-1997 outburst of the GRO J1655-40 in SPL state, the jet was not observed (Tomsick et al. 1999). The similar behavior was observed in the Cyg X-1 in its transition from the low hard state to very high state (Gallo et al. 2003; Tigelaar et al. 2004). But while XTE J1550-564 was very bright, the Chandra X-ray images revealed strong powerful jets from the source as a result of optically thin synchrotron emission (Corbel et al. 2002; Kaaret et al. 2003; Tomsick et al. 2003).

2.1.5 Intermediate State

The intermediate state links the low hard state and SPL states. It represents the transition between hard and thermal dominated states. It consists of the both soft and hard component of the X-ray spectrum with low emission rates. The band limited power law continuum and accretion disk contribution are usually seen in the spectrum (Mendez & Van der Klis 1997).

2.2 ACCRETION MECHANISMS IN X-RAY BINARIES

Until the discovery of Sco X-1 in June of 1962, the process of accretion had little attention in astrophysics. Shyklovsky suggested first in 1967 that the X-ray binaries are driven by the accretion from the companion onto compact star

(Carpenter et al. 1977). The accretion process then applied to binary systems which consist of compact objects; white dwarfs and active galactic nuclei. Two kinds of accretion mechanism are observed in X-ray binaries; accretion by Roche Lobe overflow and by stellar wind.

2.2.1 Accretion via Roche Lobe Overflow

After a certain stage of the evolution, the star fills its Roche Lobe and the matter begins to flow through the inner Lagrangian point from companion star to compact star. We may assume that most of the inflowing matter accretes. The outflowing matter is the stream of plasma which is transferred from inner Lagrangian point through the accretion disk. The outflow begins to form a radius where the radiation pressure and gravitation forces are comparable and pressing the matter to the plane of the disk. There is a bright hot spot where the plasma meets the accretion disk. Accretion via Roche Lobe overflow is more efficient than accretion via stellar wind. In the disk fed systems, all of the material accreting from the companion is captured by the compact star. On the other hand, in the wind fed systems, the small fraction of the wind is captured by the compact star and the mass spreads in all directions.

2.2.2 Accretion via Stellar Wind

In most of the X-ray binaries, the high mass companion ($M \geq 2.5 M_{\odot}$) does not fill its Roche Lobe and it accretes via stellar wind. The companions are O and B giants or supergiants. In wind-fed X-ray binaries, small fraction of the wind

is captured by the compact star and falls into the sphere under the influence of the strong gravitational field of the black hole. In the presence of the angular momentum of the accreted material of the black hole, the matter is prevented from falling directly onto the black hole (see Figure 2.2). At some distance from the black hole material rotates, in a circular orbit and forms an accretion disk where the centrifugal forces are comparable to gravitational ones. The matter rotating in the accretion disk falls into the black hole if it loses angular momentum ensured by the viscous forces in the disc. The viscosity has two effects. First the viscosity transports the angular momentum outward, thus allows the material spiral in toward the central mass. At the same time viscosity acts as a frictional force which results in a dissipation of heat. Some of this heat is radiated and leading to the observed spectrum. The material in the accretion disk drifts inward up to the innermost stable circular orbit ($r_{ISCO} = 3R_{shw} = 6\frac{GM}{c^2}$) about the black hole. At this point the matter spirals into the black hole (Longair 1992). While the matter spirals down to black hole, gravitational potential energy is released. Part of this energy raises the kinetic energy of the rotation and the other part is inverted into thermal energy and radiated from disk surface.

The total energy release is determined by the accretion rate of the matter into the disk. The value of flux of matter $\dot{M}_{cr}$ which the total release of energy in the disk $L = \eta \dot{M}_{cr} c^2$ is equal to the Eddington critical luminosity

$L_{cr} = 10^{38} \frac{M}{M_\odot}$ergs s^{-1} , characterized by the equality of the force of radiation pressure on the completely ionized matter and of the gravitational forces of attraction to the star (η is the efficiency of gravitational energy release, in the case

of Schwarzshild's metric $\eta \approx 0.06$ in a Kerr black hole η can attain 40 %).

$$\dot{M} = 3 \times 10^{-8} \frac{0.06}{\eta} \frac{M}{M_\odot} \frac{M_\odot}{year} \tag{2.1}$$

When the inflow of the matter to the disk exceeds the critical value, the subcritical value accretion rate is possible. At the subcritical fluxes $\dot{M} \approx 10^{-12} - 10^{-10} M_\odot \text{year}^{-1}$ the luminosity of the disk is in the order of $L \approx 10^{34} - 10^{36} \text{ergs s}^{-1}$ and the surface temperature is the order of $T \sim 3 \times 10^5 - 10^6$ K in the inner regions of the disk where the most of the energy released. This energy radiated

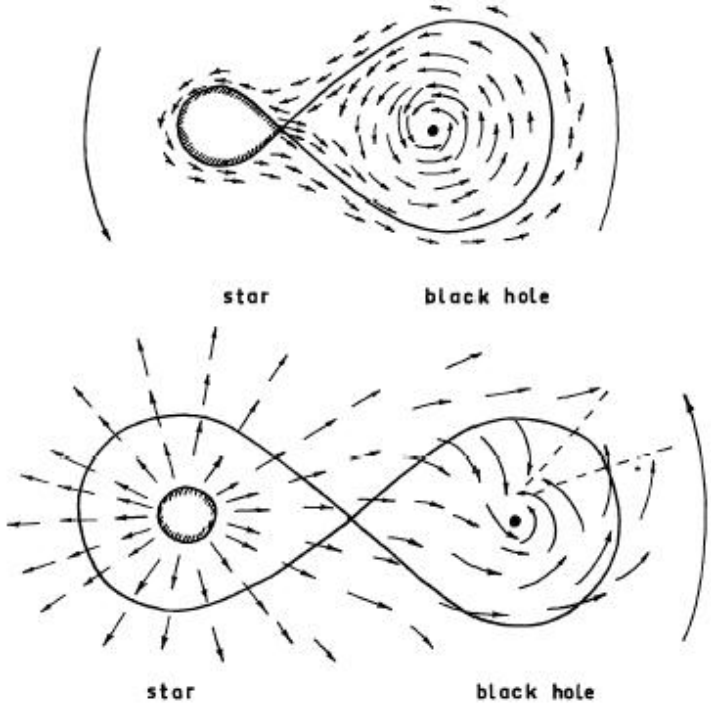

Figure 2.2: Two regimes of matter captured by a collapsar: a) a normal companion fills up its Roche lobe, and the outflow goes through the inner Lagrangian point; b) the companion's size is much less than Roche Lobe the outflow is connected with a stellar wind. The matter loses part of its kinetic energy in the shock wave and thereafter, the gravitational capture of accreting matter becomes possible (Shakura & Sunyaev 1973).

in the ultraviolet and soft X-ray bands.

The wind passing within a cylindrical radius accretes from compact star moving with orbital velocity in a stellar wind of velocity ν_w;

$$r_{acc} = \frac{2GM}{v_{rel}^2} \tag{2.2}$$

where $v_{rel}^2 = v_w^2 + v^2$ If the wind is emitted over solid angle Ω and has a total mass-loss rate $\dot{M}_w$ this implies an accretion rate

$$\dot{M} \approx \frac{\pi r_{acc}^2}{4\pi a^2} \dot{M}_w \tag{2.3}$$

where a is the binary separation. In the isotropic wind case in OB supergiants, high velocities $v_w = 1 - 2 \times 10^3$km s^{-1}, $r_{acc} \approx 10^{10}$ cm, a $\approx 10^{12}$ cm, the mass loss rate is in the order of $\dot{M} \approx 10^{-4} M_\odot$ (King, Van Paradijs 1995).

2.2.3 Disk Formation

Some X-ray binaries are close enough binaries and generally thought to be accreting material through Roche Lobe overflow. The matter passing through the inner Lagrangian point spirals through the accretion disk by losing angular momentum and it accretes to the central compact object. The thermal bremsstrahlung process in the inner disk is responsible for the X-ray radiation with effective temperature $\approx 10^5 - 10^6$ Kelvin. The X-ray flux primarily depends on the mass transfer rate $\dot{M}$. If the specific angular momentum J of the accreting matter in the disk is too large to hit the accreting object with mass M_1, it forms a disk. This holds for the circulation radius

$$R_{circ} = \frac{J^2}{GM_1} \tag{2.4}$$

This equation holds for low-mass XRBs which accrete via Roche Lobe overflow. The picture is unclear when the accretion is via wind flow (King, van den Heuvel, 1995).

In the case of disk accretion the radiation intensity depends on the frequency; $\nu^{-1\div+1/3}$ at $h\nu < kT_{max}$. As a result the optical part of the luminosity is considerable. For a M=$10M_{\odot}$ black hole even $\dot{M} = 10^{-9}M_{\odot}$ year^{-1} the optical luminosity is of the order of the average solar value. The irradiation of the hard radiation of hot central regions of the disk is responsible for X-ray radiation. The outer region of the disk is thick enough to absorb the X-ray radiation and reradiate the absorbed energy up to 0.1-10 % of the total luminosity in ultraviolet and optical bands. The non-thermal radiation mechanisms' existence strongly depends on the magnetic field strength of the order of $\approx 10^5 - 10^7$ Gauss (Shakura & Sunyaev 1973).

2.2.4 Quasi-Periodic Oscillations (QPOs)

Most of the bright galactic bulge sources exhibit transient intensity variations called quasi-periodic oscillations. Together with the X-ray spectroscopy, studying rapid aperiodic and quasi periodic variability lead us to obtain information about physical processes in the vicinity of the compact object. The QPO behavior is thought to be correlated with the spectral X-ray states, namely the horizontal, flaring and normal branches in neutron star systems. The horizontal, normal and flaring branches have frequencies of QPO in the range $\approx$ 20-55 Hz and 7-20 Hz respectively. But the black hole candidates show evidence to have much lower

frequency QPOs. GX 339-4 has the centroid frequency around 3-8 Hz (Miyamoto et al. 1991) and GRO J1655-40 has frequency around 0.1-7 Hz (Remillard et al. 1999b). Several models have aimed to understand the QPO behavior. Among them the Beat Frequency Model is the most precise model which explains the horizontal branch kilohertz QPOs and X-ray pulsar QPOs (Alpar & Shaham 1985). There is no hard surface which rotates at a different speed than the inner edge of the disk. Hence there is no model that can explain all the apparent features correlations in the QPO phenomenology. The features of these models are the followings: In the viscous pulsational instability model, the oscillation is thought to be excited by axially symmetric acoustic modes at the transonic region of the disk close to the black hole. The frequency of the oscillation is about $10^3(M/M_\odot)^{-1}$ Hz. The observed QPO frequency is too low with respect to the found value (Kato 1988). The other mechanism used for explaining the QPO phenomenology is "one armed corrugation wave" generation the inner edge of the disk where the disk oscillates vertically as a whole. The frequency of the oscillation is around 1-0.002 Hz for critical accretion rate but the problem with the observed modulation persist.

Another mechanism involves the trapped oscillations which are generated closer to the inner edge of the accretion disk. These oscillations appear as there is a maximum in the epicyclic frequency. These oscillations show 1-3 % modulation in the absence of accretion. The computation which includes accretion is to be performed in order to find the relevance of these modes (Nowak & Wagoner 1993). The final mechanism is due to oscillation of shock waves close to the black hole.

Centrifugally supported shock waves perform as hard surface and the post-shock flow produces hard radiations. When the cooling time of this region agrees with the in-fall time, the shock oscillates, modulating the hard-radiation by 5-15 % (Chakrabarti & Molteni 1995).

2.2.5 Low Frequency QPOs (LFQPOs)

In the range of 0.1-30 Hz the X-ray power density spectrum shows low frequency QPOs and seen in the steep power law state (SPL). They are generally seen above 60 keV (Tomsick & Kaaaret 2001). While The LFQPOs are observed with rms $0.03 < r < 0.15$, ones in the range with rms amplitudes r $\geq$0.15 are extremely strong for source GRS 1915+105 (Morgan et al. 1997) and XTE J1550-564 (Sobczak et al. 2000a). In several sources flux and LFQPO frequency correlation is observed (Sobczak et al. 2000a; Menou et al. 1999; Trudolyubov et al. 1999). This significant feature is consistent with the theory which proposes that the SPL component and thermal component are coupled (McClitock & Remillard 2004). LFQPOs can be quasi stable features which persist for days and months. In GRS 1915+105, 2.0-4.5 Hz range QPOs persist for 6 months during late 1996 and early 1997 (Muno et al. 2001).

The models which try to explain LFQPO mechanism include global disk oscillations (Titarchuk & Osherovich 2000), radial oscillations of accretion structures such as shock fronts (Chakrabarti & Manickam 2000) and oscillations in a transition layer between the hotter Comptonising region and the disk (Nobili et al.

2000). Another model is accretion-ejection instability model which executes spiral waves in a magnetized disk (Tagger & Pellat 1999) with a transfer of energy out to the radius where the matter correlates with spiral wave (McClitock & Remillard 2004).

2.2.6 High Frequency QPOs (HFQPOs)

The BHBs GRS 1915+105 and GRO J1655-40 are subject to the first detections of fast X-ray variability thought to be signatures of strong-field GR effects in the inner accretion disk. The first discovered HFQPO in GRS 1915+105 was 67 Hz QPO by RXTE (Morgan, Remillard and Greiner 1997).

High-frequency QPOs are (40-450 Hz) are generally seen in the SPL state but 67 HZ QPO seen in the GRS 1915+105 is the feature of the thermal dominated (high-soft) state. They have rms amplitudes $\sim 1-3\%$ of the mean count rate in a given energy band (McClitock & Remillard 2004). 3 BHB and 4 black hole candidates (BHC) exhibit pair of QPOs that have commensurate frequencies $3 \div 2$ ratio (Remillard et al. 2002b; Remillard et al. 2003b). GRO J1655-40, XTE J1550-564 and H 1743-322 exhibit twin QPOs at frequencies 300-450 Hz (Remillard et al. 1999b), 184-276 Hz (100-184 Hz; Remillard et al.1999a; Homan et al. 2001 ; Homan et al. 1999c) and 160-240 Hz (240 Hz; McClintock and Remillard 2004) respectively. Additional single HFQPOs were found in the, XTE J 1859+ 226 (150-187 Hz; Cui et al. 2000a), XTE J1650-500 (250 Hz; Groot et al. 2001) recurrent BHC transient 4U 1630-47 (184 Hz; Remillard et al. 1999a,b). In addition the source GRS 1915+105 possesses a pair of HFQPOs (67 Hz + 41 Hz)

which actually show up during the HS state. These QPO frequencies do not vary with the X-ray flux; they are a fingerprint of the system (Morgan et al. 1997; Remillard and Morgan 1999)

The high frequency QPOs are similar to the innermost stable circular orbit (ISCO) frequencies in stellar mass black holes. The theory on discoseismic modes is candidate for explaining constant frequency of HFQPOs but is weak to predict harmonic sets of frequencies in HFQPOs (Nowak et al. 1997; Perez et al. 1997; Wagoner & Ortega-Rodriguez 2001; Silbergleit et al. 2001). Other models must be considered as well, p-modes oscillations of an accretion torus surrounding a black hole is a successive model for predicting integer frequency ratios. Cui et al. (1997b) propose that high frequency QPOs occur at nodal frequency. Relativistic resonance models predicted constant frequencies in small integer ratios seen in GRO J1655-40 (Strohmayer 2001a; Abramowicz and Kluzniak 2001).

Those fast QPOs are produced in the inner accretion disk (ISCO) near the black hole event horizon in which general relativity effects are noticeable and QPO frequency depends on both the spin and mass of the black hole. The strong similarities exist between the kilohertz QPOs observed in the low magnetic field neutron stars and high frequency QPOs seen in black hole candidates (Psaltis et al. 1999).

2.2.7 Kilohertz QPO Models

Most of the models which propose an explanation for kilohertz QPOs involve the orbital motion of the neutron star. The first kilohertz QPO (kHz QPO) model

was magnetosperic beat-frequency model (van der Klis et al. 1996b, Strohmayer et al. 1996c). But it has not been applied much to kHz QPOs (Cui et al. 1997). The most prominent one is sonic point beat frequency model (Miller et al. 1996; Miller et al. 1998a), but relativistic precession model (Stella and Vietri 1998; 1999), photon bubble model (Klein et al. 1996) have been also notable ones.

The sonic point model was modified and based on beat frequency model (Lamb and Miller 1999; Miller 1999). In the sonic point beat frequency model the sonic radius r_{sonic} where the velocity of the radial inflow is supersonic is defined near the innermost circular stable orbit r_{ISCO}. Then matter and clumps follow a spiral orbit around the neutron star. At the "footpoint" where the matter hits neutron star surface the emission is enhanced. The footpoint travels around the surface at clumps' orbital velocity so the hot spot is observed moving with Keplerian frequency around the neutron star at r_{sonic}. According to Miller (1999), this produces upper kHz QPO ν_u . The beat frequency ν_{beat} is generated by the matter that accretes onto the neutron star magnetic poles and sweeps around neutron star spin frequency ν_{spin}. It irradiates the clumps at r_{sonic} once per beat period. This beat frequency $\nu_{beat} = \nu_\phi(r_{sonic}) - \nu_{spin}$ is called lower kHz QPO frequency ν_l.

Contrary to the observations, the sonic point beat frequency model predicts that $\Delta\nu = \nu_u - \nu_l = \nu_{spin}$. As the matter spirals down to the neutron star, the observed beat frequency would be higher than the actual beat frequency. Because the lifetime of the clumps diminish while the clumps spiral through the neutron star's surface. Also the orbital frequency would be lower than the actual orbital

frequency as the angle between the clump and footpoint is getting smaller. Thus the lower kHz QPO frequency is closer to the upper one and $\Delta\nu$ decrease, at higher luminosity due to strong radiation drag the spiraling down is faster (Lamb and Miller 1999; Miller 1999).

The free-particle orbiting around a spinning neutron star shows both relativistic periastron precession (Einstein 1915) and nodal precession due to relativistic frame dragging (Lense & Thirring 1918). In the relativistic precession model the upper kilohertz QPO frequency ν_u is identified with the orbital frequency ν_ϕ which is the frequency of the orbit at the inner edge of the disk ν_l (10-100 Hz). Lense-Thirring precession frequency ν_h is related to the nodal precession frequency ν_{nodal} and periastron precession frequency ν_{peri} (Stella and Vietri 1998, 1999). In the model ν_h is proportional to ν_ϕ^2 and ν_u^2. This result is consistent

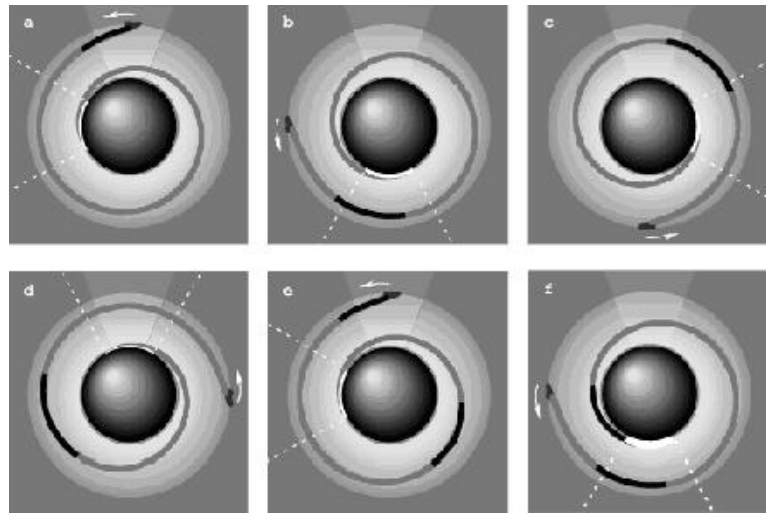

Figure 2.3: The clump's spiral motion around the neutron star and the footpoint emission (Miller et al. 1998).

with the observations. Also the QPO peak separation is proportional to ν_u. The relativistic precession model fails to explain why $\Delta\nu$ is the equal to the star's spin frequency. To get a more precise match between the model and observations, additional free parameters are required. For a detailed explanation about the model see Psaltis et al. (1999) and Markovic & Lamb (1998, 2000).

Photon bubble model is used to explain QPO phenomena without including rotational effect (Klein et al. 1996). This model is based on numerical radiation hydrodynamics. Matter accretes along magnetic funnel within which accretion is Super-Eddington so that photon bubbles form which rise up by buoyancy and burst at the top in quasi-periodic sequence (van der Klis, 2000).

Even QPO phenomena in black holes and neutron stars are completely different, some theories explain them in a similar way. In black hole binaries, QPOs are generally seen as single with high harmonics and stable whereas in neutron star binaries they are observed in pairs with low harmonics and they have variable frequencies. Because the QPOs form at variable radius which is set by interaction of the disk flow with magnetic field and radiation from the stellar surface, their frequencies are also variable in neutron star systems. But in the black hole binaries due to the negligible effects of these features QPO phenomena form in almost stable orbit ISCO. The second kHz QPO occurring in neutron star systems is a consequence of an interaction of the disk flow with star spin. The relativistic effects on the flow may results in the high QPO harmonics in black hole systems.

2.3 JETS FROM X-RAY BINARIES

Relativistic particle outflow namely jet phenomenon is one of the most significant features of the X-ray binaries. In 1960s and 1970s, Sco X-1 (Hjellming & Wade 1971a), Cyg X-1 (Hjellming & Wade 1971b) and the outbursting source Cyg X-3 (Gregory et al. 1972) were known to be radio sources. In 1979, with the discovery of X-ray binary SS 433 (Spencer 1979; see also Hjellming & Johnston 1981), X-ray binary jets opened up as a new research area. In the 1990s after the discovery of the microquasar GRS 1915+105 (Mirabel & Rodriguez 1994; see also Mirabel & Rodriguez 1999; Fender et al. 1999a; Rodriguez & Mirabel 1999; Fender et al. 2002), it was understood that X-ray binaries exhibit highly relativistic jet outflow (Lorentz factors $\tau \geq 2$, where $\tau = (1 - \beta^2)^{-1/2}$ and $\beta = v/c$). Shortly afterwards GRO J1655-40 was discovered as galactic superluminal black hole binary which also displays highly relativistic particle outflow (Tingay et al. 1995; Hjellming & Rupen 1995).

2.3.1 Jet Formation

The jet formation process has not been explained clearly yet. But there are several theories which try to explain the mechanisms of jet formation.

Blandford and Payne (1982) argued in their model that the magnetic fields in accretion flow may produce radio loud jets. Meier (2001) and Koide & Uchida (2001) have predicted the contribution of low-hard state in MHD jet formation. In this interpretation, the jet formation is the feature of the low-hard state. As the

source goes into its high-soft state, the radio jet formation is suppressed. Livio, Pringle & King (2003) interpreted a model in which hard X-states represent the modes. for these modes, the bulk accretion energy is converted into the bulk motion of the relativistic jet. Fender, Gallo & Jonker (2003) verify this proposal of the observations. The formation of jets with the contribution of the magnetized accretion disk which is based on the MHD outflow is proposed by Lynden-Bell (2003). This theoretical model has been given widespread acceptance of magneto-rotational instability (MRI) as the origin of accretion disc viscosity (e.g. Balbus & Hawley 1991; Turner, Stone & Sano 2002). In the accretion-ejection instability model, the vertical component of the inner accretion disk may transport the energy and angular momentum as powering jet or wind (Varniere & Tagger 2002). This model purposes that the X-ray timing features of accretor and the jet couples (Das, Rao & Vadawale, 2003; Nobili, 2003). In addition to the magnetic acceleration, the radiative acceleration is also a mechanism to power the jets away from the accretion disk (Phinney, 1982). Rees et al. (1982) was put forward a model which discusses the connection between the "ion-supported tori" and formation of radio jets (Fender, 2003).

2.3.2 Radio Emission From X-ray Binaries

The key property of jet formation of X-ray binaries is the synchrotron emission (Mirabel & Rodriguez 1999; Fender 2005). For more extended explanation about syncrotron radiation see Longair 1992.

Different X-ray states are associated with different jet structures (see Figure

2.4); steady jets and transient jets (Fender 2005).

Steady jets display persistent radio emission with flat radio-mm spectrum. The emission lines in the spectrum are the indications of the continuous emission from relativistic plasma. The flat spectrum results from the synchrotron emission from partially self-absorbed, steady jets which are more transparent to the low frequencies as the particles travel away from the launching site (Blandford & Knigl 1979; Hjellming & Johnston 1988; Falcke & Biermann 1996). This phenomenon

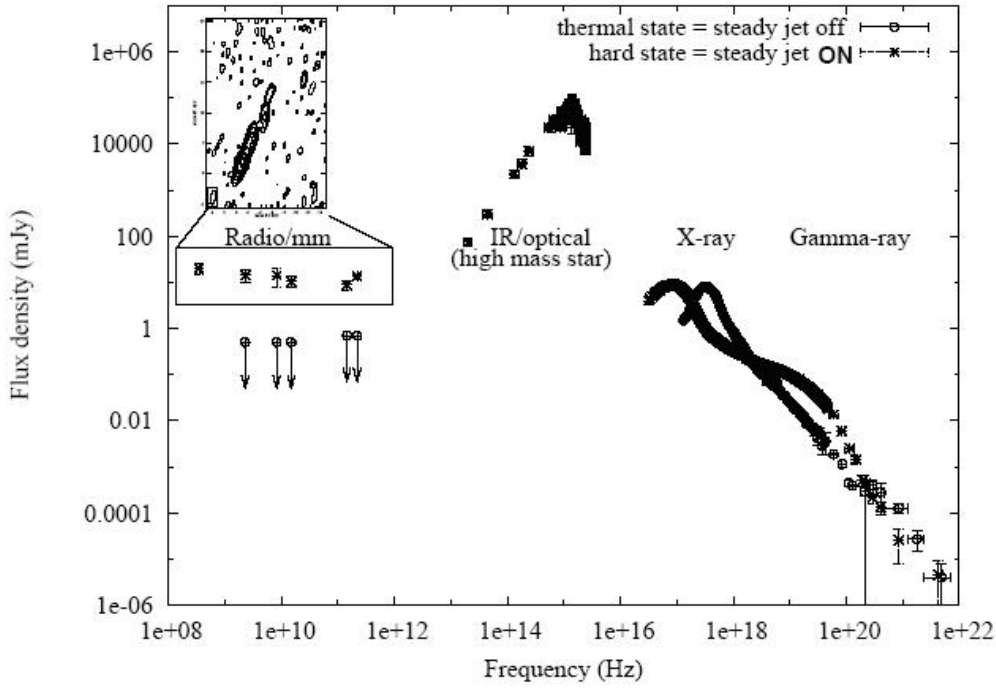

Figure 2.4: Spectral energy distribution of Cyg X-1 with 10 $M_{\odot}$ over different accretion regimes. When the hard (above 1018 Hz) X-ray spectrum is dominated by a hard power-law component, the system is persistently detected in the radio band. The radio-mm spectrum is flat, due to a partially self-absorbed steady jet resolved on milliarcsec-scales. Above a critical X-ray luminosity of a few per cent Eddington, the disc contribution becomes dominant, while the hard X-ray power law softens (Gallo & Fender 2005)

is called steady jets see Figure 2.5. Characteristics of the hard state jets of Cyg X-1 (Stirling et al. 2001) and GRS 1915+105 (Dhawan et al. 2000; Fuchs et al. 2003) are consistent with the milliarcsec (tens of A.U.) collimated jets. The long term accretion infers collimated jets, hard state of BHXBs 1E1740.7-2942 and GRS 1758-258, both associated with arcmin-scale radio lobes (Rodriguez et al. 1992; Marti et al. 2002). Markoff, Falcke & Fender (2001); Markoff et al. (2003) interpret that the jet formation is associated with the hard/ quiescent state of which the X-ray spectrum is dominated by the power law. In the model, the jet synchrotron emission is optically thin to self absorption and synchrotron self-Compton emission.

Radio emission is suspended in the soft (thermal dominant) state, so the jet

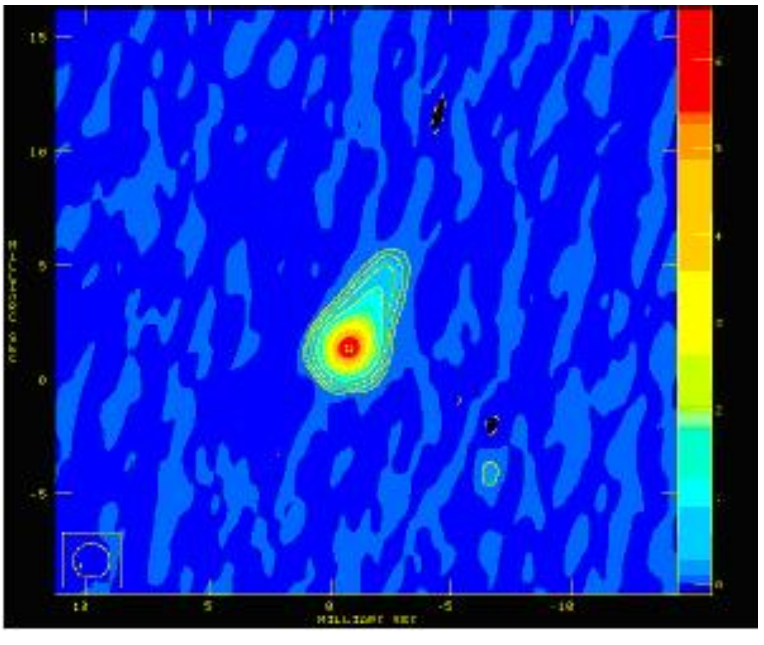

Figure 2.5: Image of steady jets structure of Cygnus X-1 from 1997 March 28 (Stirling et al.2001)

disappears (Fender et al. 1999; Corbel et al. 2001).

VLA observations of GRS 1915+105 in 1994 proved that the BHBs produce relativistic jets (Mirabel & Rodriguez 1999). Relativistic particles move away from the black hole by emitting synchrotron emission during transition between the X-ray states (Mirabel & Rodriguez 1994, 1999; Fender et al. 1999). These emissions are optically thin synchrotron emission. The transient radio ejection is due to the expansion losses. The monotonic decay is observed few days after the transient ejections (primarily due to adiabatic losses) as the decay rate is the same at all frequencies. The synchrotron emission or inverse Compton scattering is the result of more rapid decay in higher frequencies. The observed synchrotron emission from these events is small fraction of the energy input. This kind of phenomena is called as transient jets (Fender 2005). The transient jet structure of GRS 1915+105 jet is shown in Figure 2.6.

2.3.3 Disk-Jet Correlation

The term disk-jet coupling refers to the relation between inflow and outflow. The flat radio spectrum is observed in low-hard state which is associated with the jet formation in the core. BHB states serve us to understand the behavior of the accretion mechanism. These states are also indications of the jet formation.

In low-hard state and quiescent state, the X-ray spectrum is dominated by the power law component (broadband) which has photon index ~ 1.7 with a cut-off around 100 keV. The spectrum also includes the accretion disk component of weak black body and a relatively weak gamma ray tail. It shows up 40 % rms

variability with a break around few Hz. The radio spectrum in low-hard state and variability correlated with the X-ray flux. These properties are different from those found in the transient ejections (Fender 2001). By comparing with AGN jets, it could be explained as they are self-absorbed, compact, steady jets (Hjellming & Johnston 1988; Falcke & Biermann 1996, 1999; Fender 2001; see also Blandford & Konigl 1979). The hard state associated with milliarsec-scale jet of GRS 1915+105 show similar behavior see Figure 2.6 (Dhawan, Mirabel & Rodriguez 2000).

The correlation between radio and X-ray fluxes was first observed by Hannikainen et al. (1998) for GX 339-4. Similar behavior observed in Cyg X-1

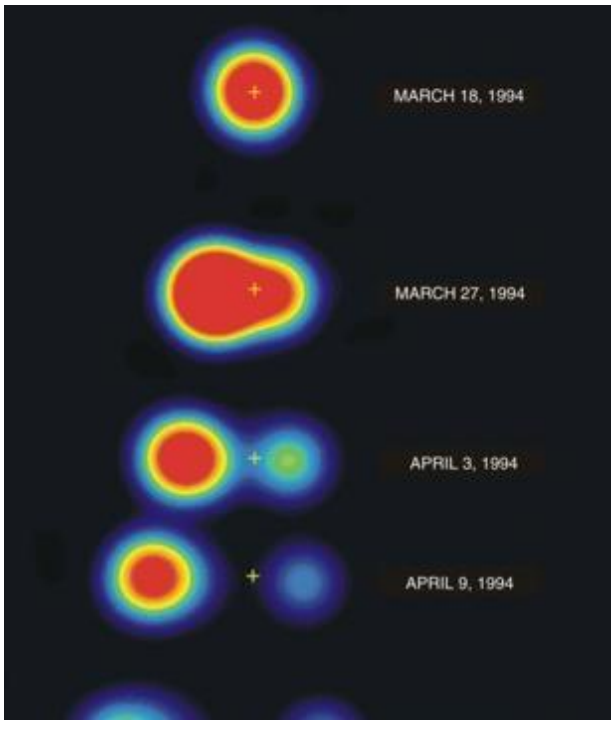

Figure 2.6: Transient jet structure of GRS 1915+105 (Mirabel & Rodriguez 1994)

(Brocksopp et al. 1999) and Fender (2001) interpreted that the magnitude of the radio and X-ray fluxes similar for all low-hard state BHBs. The luminosities in the X-ray band and radio band was found as $L_{radio} \propto L^{b}_{X-ray}$ where $b \sim 0.7$ for X-rays up to at least 20 keV for GX 339-4 (Corbel et al. 2000, 2002). The bulk Lorentz factor of low-hard state jets is $\tau < 2$. Furthermore by compling of data for ten low-hard state sources, it was found that the luminosity range $10^{-5} L_{Edd} < L_x < 10^{-2} L_{Edd}$, above this level radio emission is rapidly quenched.

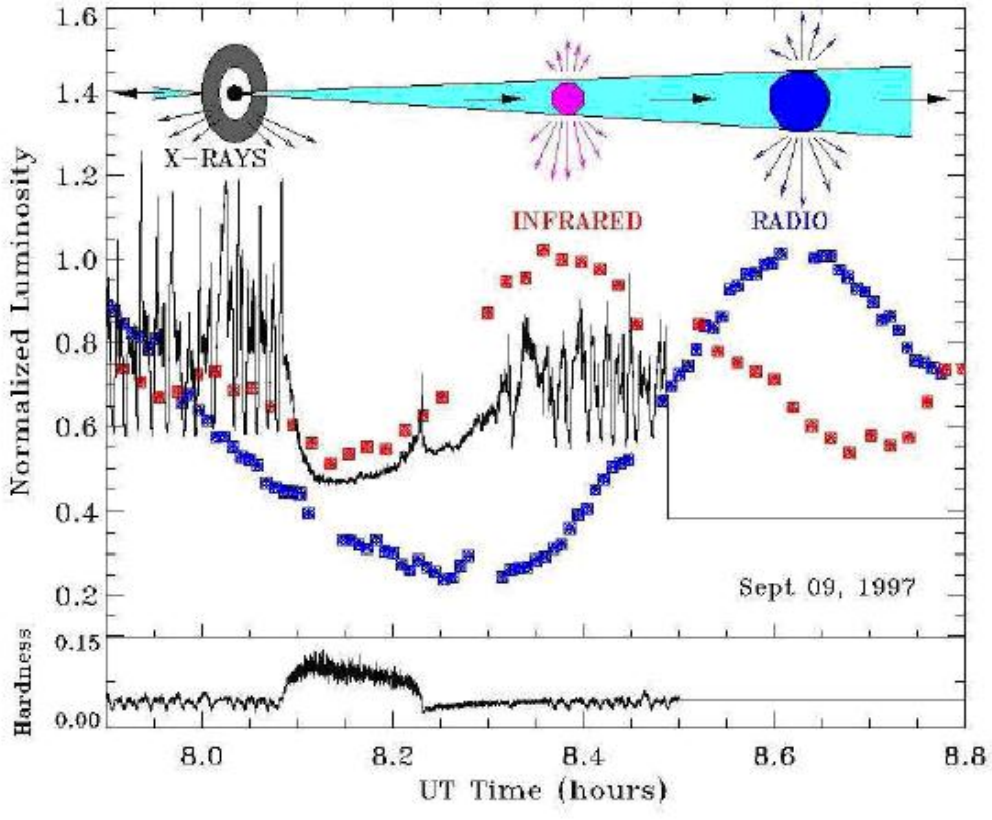

Figure 2.7: Radio, X-ray and infrared light curves of GRS 1915+105 at the time of QPO with scales of time 20 min (I. F. Mirabel, V. Dhawan, S. Chaty, L. F. Rodriguez, J. Marti, C. R.Robinson, J. Swank, T. Geballe, A & A 330, L9 1998). The infrared flare starts during the recovery from the X-ray dip, when a sharp, isolated X-ray spike-like feature is observed.

The velocity of the jet in low-hard state is simply $\beta = v/c \leq 0.8$ (Gallo et al. 2003).

BHBs stay in quiescence state with the luminosity range $10^{-6} - 10^{-9} L_{Edd}$ (Garcia et al. 2001). The X-ray spectrum is very similar to the spectrum of the low-hard state with powerful jet formation. Combining with the estimates of jet power in low-hard state with $L_{radio} \propto L^{0.7}_{X-ray}$ relation indicates that quiescent BHCs will in fact be jet dominated in the sense that most of the power output will be in the form of an outflow (Fender, Gallo, Jonker 2003).

Most of the transient sources are brighter in X-ray luminosity in their low-hard state then make a transition to the high state while shock form in a previously generated steady jet through the faster moving SPL state jet. The shock scenario is discussed first for GRS 1915+105 by Kaiser, Sunyaev & Spruit (2000), Vadawale et al. (2003) and Türler et al. (2004). Internal shocks explain why the transient emissions are optically thin unlike the steady jets which form it. The strength of the jet is related to the amount of the material lying in the path of faster SPL jet.

The very high state is referred to as hybrid state. It resembles intermediate state in its X-ray hardness between soft and hard state which are stable states (McClintock & Remillard 2004). This state is rarer than soft or high state. The radio properties of the SPL state is complicated. GS 1124-683 spent in its extended time in very high state. Rapid changes in the accretion disc radius correspond to discrete ejections. During its very high state, the bright and variable radio emission was observed (Miyamoto et al. 1993; Kuulkers et al. 1999),

whereas in the brightest days of GRO J1655-40 during 1996-1997 outburst and 1996 August SPL state, no radio emission was observed (Tomsick et al. 1999). Similarly Cyg X-1 appeared radio quite whenever it makes transition from low state to SPL state (Gallo et al. 2003; Tigelaar et al. 2004). But observations of XTE J1550-564 confirm that the radio jets switched on throughout SPL state (Hannikainen et al. 2001). From these evidences, we may say that the SPL state is essentially radio quite but the instabilities may cause relativistic jet ejections (McClintock & Remillard 2004).

In the high-soft state radio jet formation was detected (Tananbaum et al. 1972) in the transition of Cyg X-1 from soft state to the hard state (Hjellming, Gibson & Owen 1975). GX 339-4 spent a year in its high-soft state in 1998, it had a weak radio counterpart (Hannikainen et al. 1998) which could not be detected during high-soft state (Fender et al. 1999, Corbel et al. 2001). When it evolved through the hard state, the radio counterpart appeared again (Corbel et al. 2000). It is strongly evidenct that the radio emission disappear in soft state (see Figure 2.7).

CHAPTER 3

RXTE OBSERVATIONS AND DATA ANALYSIS

3.1 RXTE Observations

The Rossi X-ray Timing Explorer (RXTE) named after astronomer Bruno Rossi observes for cosmic X-ray sources and their variability over time scales ranging from milliseconds to years by making sensitive measurements. It was launched on December 30, 1995 with 3000 kg mass. It is sensitive to energy range 2-200 keV. RXTE carries three instruments; the High Energy X-ray Timing Experiments (HEXTE) (Gruber et al. 1996), the All Sky Monitor (ASM) (Levine et al. 1996) and the Proportional Counter Array (PCA) (Jahoda et al., 1996).

HEXTE is sensitive energies up to 200 keV. ASM scans the sky every 1.5 hours in the energy range 2-10 keV monitoring long-term behavior of a number of the brightest X-ray sources and allows the observer to spot any new phenomenon quickly. PCA has five xenon gas proportional counters with a total collecting area of 6500 cm^2 in the energy range 2-60 keV. The time resolution of the PCA is 1 microseconds and the field of view 1 square degree. Events detected by the PCA are processed on board by the Experiment Data System (EDS), a microprocessor driven-on-board data system before insertion into the telemetry stream. The EDS is capable of processing up to 500000 counts per second. The data is collected in

variety of different data modes simultaneously.

3.2 The Fourier Transform

In calculating power spectra, Fourier transform was used. Fourier transform is an operation which converts functions from time to frequency domain. At any given frequency, the infinitely extended continuous function *x(t)* can be expressed as;

$$x(t) = \frac{1}{N} \sum_{j=-N/2}^{N/2-1} a_j \cos(w_j t - \phi_j) = \frac{1}{N} \sum_{j=-N/2}^{N/2-1} A_j \cos(w_j t) + B_j \sin(w_j t) \quad (3.1)$$

where A_j and B_j are Fourier coefficients

$$A_j = \sum_{k=0}^{N-1} x_k \cos(w_j t) \quad (3.2)$$

$$B_j = \sum_{k=0}^{N-1} x_k \sin(w_j t) \quad (3.3)$$

It is seen in the equation 3.1 that A_j and B_j are the correlation of the signal *x(k)* with a *sine* and *cosine* wave of frequency w_j. In use of power spectrum x_k is stand for the number of photons detected in bin k. The discrete Fourier Transform $a_j (j = -\frac{N}{2}, ..., \frac{N}{2} - 1)$ decomposes this signal into N sinusoidal waves. The signal transform pair is in the following;

$$a_j = \sum_{k=0}^{N-1} x_k e^{2\pi i j k/N} \quad (3.4)$$

where $j = \frac{N}{2}, ..., \frac{N}{2} - 1$ and

$$x_k = \frac{1}{N} \sum_{j=-N/2}^{N/2-1} a_j e^{-2\pi i j k/N} \quad (3.5)$$

where k=0,.....,N-1. The Parseval's theorem requires that

$$\sum_{k=0}^{N-1} =\mid x^2 \mid = \frac{1}{N} \sum_{j=-N/2}^{N/2-1} \mid a_j \mid^2 \tag{3.6}$$

Adopting the normalization used by Leahy et al. (1983), the power spectrum can be defined as

$$P_j \equiv \frac{2}{N_{ph}} \mid a_j \mid^2 \; j = 0, ..., \frac{N}{2} \tag{3.7}$$

where N_{ph} is stands for the total number of photons (van Der Klis 1989);

$$N_{ph} = \sum_{k=0}^{N-1} x(k) = a_0 \tag{3.8}$$

In this thesis we investigate QPO properties of accreting black hole binaries GRO J1655-40 and GRS 1915+105. This research is based on data of GRO J1655-40 and GRS 1915+105 collected with Proportional Counter Array on board RXTE and GRS 1915+105 data which was obtained from Chandra and RXTE simultaneous observations. The data sets used in this thesis are public. We used the programs of FTOOLS version 5.2 in analysis and calculations of the data collected with RXTE. For the Chandra spectroscopy analysis, the CIAO 3.3.0.1 was used.

3.3 GRO J1655-40

3.3.1 Introduction

GRO J1655-40 is a galactic black hole binary system with a stellar mass companion. The X-ray transient GRO J1655-40 which is $\sim$ 3 kpc away was discovered with the Burst Burst and Transient Source Experiment (BATSE) on

the Compton Gamma-Ray Observatory (CGRO) on July 27, 1994 (Zhang et al. 1994). The radio jets of GRO J1655-40 were found to be moving with 92 % of speed of light (Tingay et al. 1995; Hjellming & Rupen 1995). Optical measurements made in X-ray quiescence suggest that the compact star is a black hole with mass $\approx 7.02 \pm 0.22$ $M_\odot$ and the orbital inclination $\approx 69.50 \circ \pm 0.08 \circ$ with an orbital period of 62.88 hours (Orosz & Bailyn 1997) while the companion is a main sequence star of mass $\approx 2.34 \pm 0.12$ $M_\odot$, the spectral type of the companion is F3-F6 IV (Van der Hooft et al. 1998).

Shahbaz et al. (1999) measured the rotational velocity of the companion star in GRO J1655-40 systemusing the same method as Orosz & Bailyn (1997). They found the spectral type F6 and $V_{rot} \sin i = 88.90 \pm 6.0$ km s^{-1}. Using the rotational velocity,, they have found $q = 0.387 \pm 0.05, M_1 = 6.70 \pm 1.20 M_\odot$ and $M_2 = 2.50 \pm 0.80 M_\odot$.

Israelian et al. (1999) obtained spectra of an F6 III and F7 IV star and produced synthetic spectra based on these templates assuming T_{eff} = 6,400K. Broadening both observed and synthetic spectra and comparing the result to the spectrum of GRO J1655-40, they measured $V_{rot} \cdot \sin i = 93 \pm 3 \mathrm{kms}^{-1}$.

After the discovery of GRO J1655-40 the outburst series have lasted up to late in 1997. Over this period, the source was observed several instruments on board CGRO (Harmon et al. 1995; Levinson & Mattox 1996; Crary et al. 1996; Kroeger et al. 1996; Zhang et al. 1997; Grove et la. 1998a; Hynes et al. 1998; Tomsick et al. 1999), ROSAT (Greiner, Predehl & Pohl 1995; Greiner 1996), ASCA (Zhang et al. 1997; Ueda et al. 1998), Granat (Zhang et al. 1997), Mir-Kvant (Borozdin

et al. 1997) and from 1996 RXTE (Kuulkers et al. 1998; Mendez, Belloni & Van der Klis 1998; Hynes et al. 1998b; Hynes et al. 1998c; Tomsick et al. 1999b; Sobczak et al. 1999).

In July -August 1995 the high-soft state characteristics was found in the spectrum. The power law component extended to at least 600 keV (Kroeger et al. 1996). Ueda et al. (1998) report both high-soft and low-hard state spectra. In 1996-1997 Sobczak et al. (1999) observed SPL in the first phase of the outburst, in the second phase high state and in the end low state. Mendez, Belloni & van der Klis (1998) examined the rapid X-ray variability and the transition between

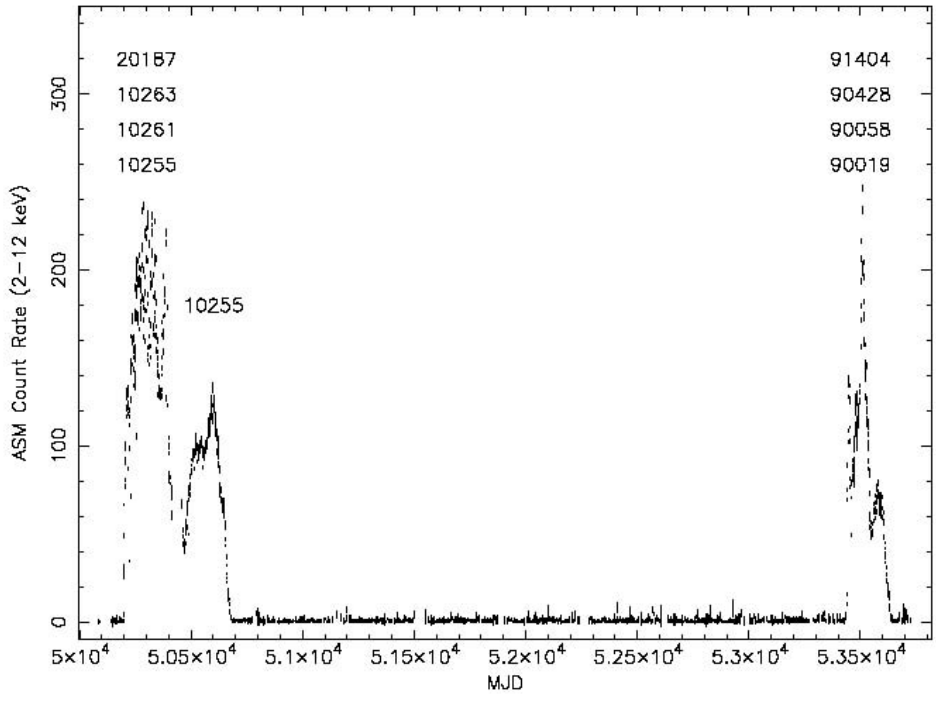

Figure 3.1: Light curve of GRO J1655-40 between 18 January 1996 and 29 July 2005 as measured with the RXTE ASM in the range 2-12 keV

the low and high states. Kuulkers et al. (1998) observed GRO J1655-40 displays short ($\sim$ 1 min) and very deep X-ray dips ($\sim$ 8 percent of the dip flux). The spectrum during a dip is dominated by absorbed component. The explanation the central black hole is covered by clumps and filaments of material above the plane of the accretion disk in the vicinity of the stream point. Remillard et al. (1999b) found the hard X-ray variability 300 Hz QPO in the low state by using RXTE observations. This feature is the result of the precession of the inner disk due to the relativistic frame dragging (Lense Thirring effect) (Cui, Zhang & Chen 1998) and discoseismic g-mode oscillations of the inner disk (Nowak & Lehr 1998). All of these models interpret that the central black hole is rapidly spinning (80 % of maximum).

Radio observations in 1994 showed that the radio flux was correlated with the hard X-ray flux but with declining amplitude (Tingay et al. 1995; Hjelming & Rupen 1995). The velocity of these highly relativistic jets was 0.92 % of speed of light. The exact jet formation mechanism is not known but acceleration along the electric filed lines for rapidly rotating black holes proposed to explain the mechanism (Blanford & Znajek 1977). GRO J1655-40 is threaded as rapidly spinning black hole binary and the black hole spin is responsible for jet production. But during 1995 it shows no radio emission and jet structure (Hunstead, & Campebell-Wilson 1996).

3.3.2 The 1996 Outburst

Between 1995 and 1996 April GRO J1655-40 spent its time in quiescent state. In April 1996 it went into outburst (Remillard et al. 1996) throughout to the end of 1997 August. The soft X-ray flux (2-10 keV) remained constant more than four months monitored by the RXTE/ASM data whereas the hard X-ray component (20-200 keV) followed by CGRO/BATSE found increased in slow rate but it didn't reach the maximum level while until four months after the initial dramatic rise in the soft flux. Hard X-ray flux rose while the optical fluxes fall but in 1997 when the hard X-ray flux was very low optical fluxes follow soft X-rays (Hynes et al.1998).

Radio detections in 1996 outburst were short-lived. No jet was observed during the outburst. The radio flux was below the 0.5 mJy between 1996 January and May 20 (Hjellming & Rupen 1996). On May 28 the radio flux was observed (55±5) mJy (Hunstead & Campbell-Wilson (1996) and also observed at 19 mJy (Hjellmig & Rupen 1996).

The system parameters of GRO J1655-40 are best known when the companion is in quiescent. Qrozs & Bailyn (1997) proposed that main sequence companion mass is early F type subgiant star which makes a significant contribution to the optical light in outbursts with about 70 degree inclination and orbits 2.6 days around the black hole.

The binary mass function of GRO J1655-40 is determined as (3.16 ±0.15)$M_{\odot}$ (Bailyn et al. 1995b), 3.24±0.09 $M_{\odot}$ (Shahbaz et al. 1999) using quiescent data.

The distance measurement and the interstellar reddening of the GRO J1655-40 are important to calculate the absolute flux distribution. The reddening is E(B-V) =1.2±0.1 and the distance is 3.2± 0.2 kpc (Hjellming & Rupen 1995).

3.3.3 ASM Observations of GRO J1655-40

The GRO J1655-40 went into outburst two times since 1996. We have analyzed the data sets which correspond to those outbursts. Figure 3.1 shows the 1996 and 2005 outbursts and corresponding data sets. The ASM light curve and hardness ratios for 1996-1997 outburst of GRO J1655-40 are shown in Figure 3.2. The

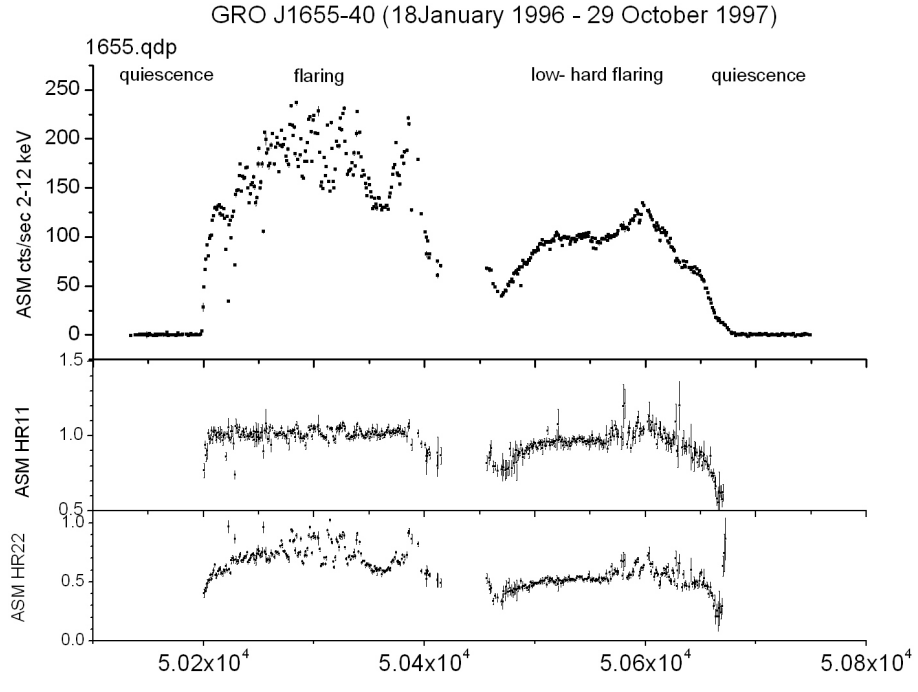

Figure 3.2: RXTE ASM light curve covering 1996-1997 outburst of GRO J1655-40

time columns are given in modified Julian date (MJD). The top panel displays the X-ray count rate at 2-12 keV versus RXTE observation dates in MJD. The bottom panels display measurements of the spectral hardness ratio HR1 which is defined as the ASM flux 3-5 keV relative to the flux at 1.2-3 keV and HR2 which represents the ASM flux at 5-12 keV relative to 3-5 keV.

We plot the ASM light curves and hardness ratios between MJD 50100 (18 January 1996) and MJD 53580 (29 July 2005) (see Figure 3.2, 3.3, 3.4). The

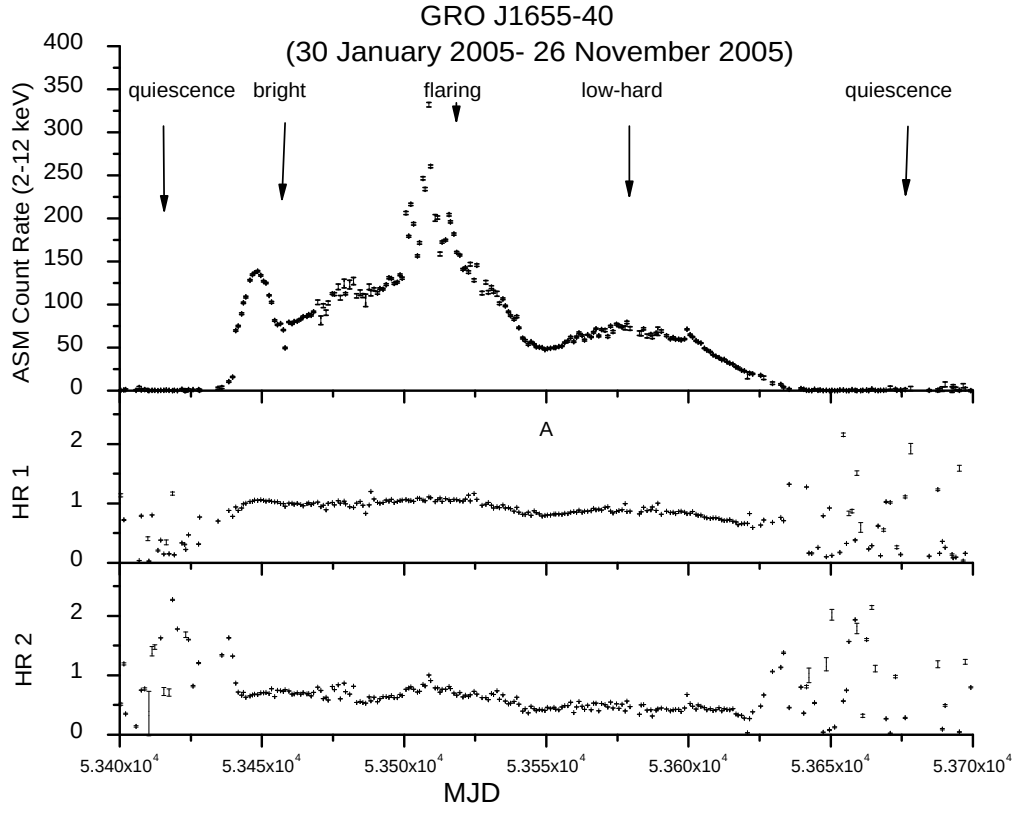

Figure 3.3: RXTE ASM light curve covering 2005 outburst of GRO J1655-40

high X-ray variability was seen in the intervals MJD 50100 and 50400 (1996 November 13) and the source evolved through very-high state see (Figure 3.2). The X-ray luminosity (unabsorbed) reached near 2×10^{38}ergs s^{-1} at 2-12 keV which corresponds to $\sim 0.25 L_{edd}$. We calculated the unabsorbed flux as $\sim 9.503 \times 10^{-8}$ergs $cm^{-2}s^{-1}$ using WebPIMMS in this time interval. After MJD 50400, the spectrum softened and the X-ray luminosity decreased until 50460 (12 January 1997) and reached to a local minimum. In the time interval between 50460 and 50560 (22 April 1997) the source seemed to be in its low-hard state and the corresponding unabsorbed X-ray flux was $\sim 6.335 \times 10^{-8}$ergs $cm^{-2}s^{-1}$. The flux rose again near MJD 50670 (10 August 1997) and reached up to $\sim 6.969 \times 10^{-8}$ergs $cm^{-2}s^{-1}$, then continued to diminish gradually until 50681 (21 August 1997) and fell below ASM detection limit (3 σ upper limits, $\sim 3.760 \times 10^{-9}$ergs $cm^{-2}s^{-1}$ per 1 day bin) (Remillard et al. 1999). Before MJD 53440 (11 March 2005) GRO J1655-40 entered its quiescent state and no flaring activity was seen. The X-ray flux rose through MJD 53440 and reached to its local maximum value after 120 days near MJD 53560 (09 July 2005). After MJD 53500 (21 March 2001), the source turned into burst once more and the corresponding flux rose up to 1.584×10^{-7}ergs $cm^{-2}s^{-1}$ then flux diminished after MJD 53550 (29 June 2005) and reached under the detection limits after MJD 53620 (07 September 2005). The hardness ratios and ASM light curve of 2005 outburst of GRO J1655-40 are seen in the Figure 3.3.

Table 3.1: Observation date and ID List of galactic microquasar GRO J1655-40

Start Date day/month/year	End Date day/month/year	XTE Obs ID	PI Name	# of Obs.
09/05/1996	26/01/1997	10255-01	Remillard	31
10/05/1996	10/05/1996	10255-02	Remillard	21
14/05/1996	30/06/1996	10261-01	Chen	12
20/05/1996	20/05/1996	10261-02	Chen	3
12/05/1996	12/05/1996	10263	Giles	1
07/11/1996	08/11/1996	20187	Robinson	1
13/03/2005	13/03/2005	90019	Spruit	1
10/02/2005	02/03/2005	90058	Swank	12
25/02/2005	03/03/2005	90428	TOO	11
04/03/2005	07/03/2005	91404	TOO	6

3.3.4 PCA Power Spectra of GRO J1655-40

We have analyzed 99 RXTE archival observations of GRO J1655-40 between 9 May 1996 and 13 March 2005 (See Table 3.1 for observation list).

We began investigating the X-ray timing behavior of GRO J1655-40 in the archive data listed in Table 3.1. We have investigated 52 RXTE pointed observations of GRO J1655-40 under the dataset ID 10255 covering 1996-1997 outburst and lasted about 450 days, 15 observations under dataset ID 10261, 1 observation for each data sets 10263, 20187 and 90019, 11 observations under proposal ID 90428, 6 and 12 observations under data sets 91404 and 90058 respectively (see Table 3.1). Totaly 99 RXTE pointed observations are investigated for GRO J1655-40 in this thesis. Remillard et al. (1999b) combined the QPO behavior and the spectral hardness. They used PCA HR1 values (the ratio of source counts at 3-5 keV relative to 1.3-3 keV). They divided the spectra into four groups. In 1996 $HR1 < 0.45$ they labelled as "soft 1996", in 1997 $HR1 < 0.45$ as "soft 1997", $0.45 <$ HR1 < 0.5 as "hard" and HR1 > 0.5 as "very hard". They suggested

Table 3.2: Significance Levels of the 300 Hz QPOs found in microquasar GRO J1655-40

Date of Obs. day/month/year	XTE Obs ID	Confidence Limits	Corresponding X-ray State
16/08/1996	10255-01-06-01	More than 5 σ (2-12 keV)	flaring
27/10/1996	10255-01-17-00	More than 3 σ (2-12 keV)	flaring

that the spectrum becomes harder as QPOs moves to lower frequencies. During soft 1997, they have reported a narrow QPO feature below 30 Hz, the 0.1 Hz QPO is in very hard group, but most important 300 Hz. Strohmayer (2001) have introduced that power spectrum also shows 450 Hz QPO property. Then they investigated whether 300 Hz and 450 Hz QPO occur simultaneously in the hard band (13-27 keV). They reported that Both 300 Hz QPO in the low energy band (2-12 keV) and 450 Hz QPOs in the high energy band (13-27 keV) were detected on 16 August 1996 and 22 August 1996, in 27 October 1996 450 Hz QPO was detected in the high energy band but 300 Hz QPO was marginally detected.

We investigated the twin QPOs both 300 Hz and 450 Hz in two energy bands low energy 2-12 keV and high energy 13-27 keV. The examined RXTE data sets are listed in Table 3.1 and retrieved from RXTE public data archive. The data set with Proposal ID P10255 consists of high resolution (sampling rate of 65,536 Hz) 16 μs event mode for photons above 13 keV corresponding to channel 35 ($\sim$ 13 keV) and 62 μs time resolution "single-bit" mode covering low energy photons in a single band (2-13 keV). Power spectra which is formed by 32s intervals and 8 Hz frequency resolution was computed for each observation and for both event mode and single-bit mode data set in the range 1 to 2048 Hz and 1 to 4096 Hz,

Table 3.3: Significance Levels of the 450 Hz QPOs found in microquasar GRO J1655-40

Date of Obs. day/month/year	XTE Obs ID	Confidence Limits	Corresponding X-ray State
16/08/1996	10255-01-06-01	More than 3 σ (13-27 keV)	flaring
01/08/1996	10255-01-04-00	More than 3 σ (13-27 keV)	flaring
22/08/1996	10255-01-07-00	More than 4 σ (13-27 keV)	flaring
04/09/1996	10255-01-09-00	More than 3 σ (13-27 keV)	flaring
09/09/1996	10255-01-10-00	More than 4 σ (13-27 keV)	flaring
27/10/1996	10255-01-17-00	More than 3 σ (13-27 keV)	flaring

respectively. We have found that QPOs near 450 Hz only are seen in high-energy event mode data whereas QPOs near 300 Hz are seen in low-energy single-bit data and we have verified that the twin QPOs ($\sim$ 300 Hz and $\sim$ 450 Hz) are also seen in certain power spectra.

To estimate the significance of the QPO feature, we modelled the power spectrum with Lorentzian and power law model (see Figure 3.6 for GRO J1655-40 and Figure 3.13 for GRS 1915+105). We normalized the power spectrum dividing it by the continuum and multiplied it by factor 2 (van Der Klis 1989). The probability of obtaining a power P= 2 $\times P_{max}\times$ number of frequency bins $\times$ number of power spectra where P_{max} is the highest power in the QPO feature (Strohmayer 2001). The $\sim$300 Hz and $\sim$450 Hz QPO features found in the data sets with IDs

Table 3.4: Significance Levels of the $\sim$300 Hz and $\sim$450 Hz QPOs found in microquasar GRO J1655-40 below $\sim 3\sigma$ confidence limit

Date of Observation day/month/year	XTE Obs ID	Confidence Limits	Corresponding X-ray State
2005-02-27	90428-01-01-03	More than 2 σ (13-27 keV)	bright
2005-03-02	90428-01-01-06	More than 2 σ (13-27 keV)	bright
2005-03-03	90428-01-01-10	More than 2 σ (2-12 keV)	bright

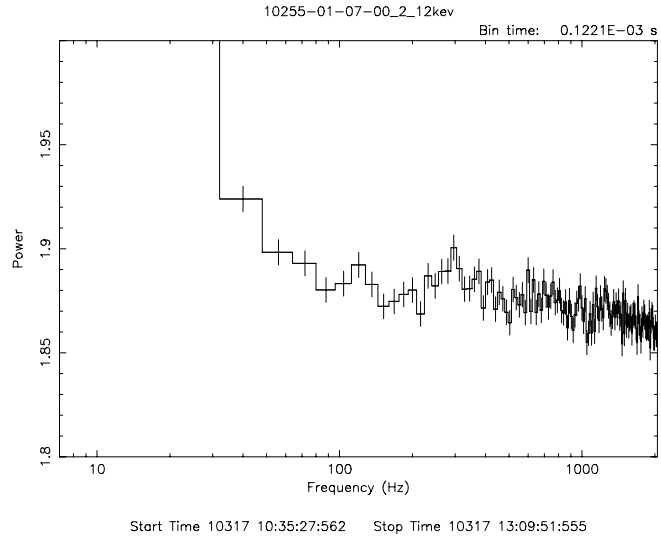

Figure 3.4: RXTE PCA power spectrum computed from the data 22 August 1996 (10255-01-07-00) of GRO J1655-40 in low energy band 2-12 keV

10255,10261, 10263, 20187, 90058, 90019, 91404 and 90408 better than $3\sigma, 4\sigma$ and 5σ confidence level is shown in Table 3.2 and 3.3, respectively. Better than 2 σ confidence QPOs are shown in Table 3.4

We have found that significant 450 Hz QPO is seen for observations 10255-01-06-01 on 16 August 1996 with exposure time 4338 sec, 10255-01-07-00 on 22 August 1996 with exposure time 13456 sec, 10255-01-09-00 on 4 September 1996 with exposure time 968 sec, 10255-01-10-00 on 9 September 1996 with exposure time 718 sec, 10255-01-17-00 on 27 October 1996 with exposure time 14891 sec. Those results are consistent with the previous results of Strohmayer (2001). Significant 300 Hz QPOs are seen in the data sets which are consistent with the

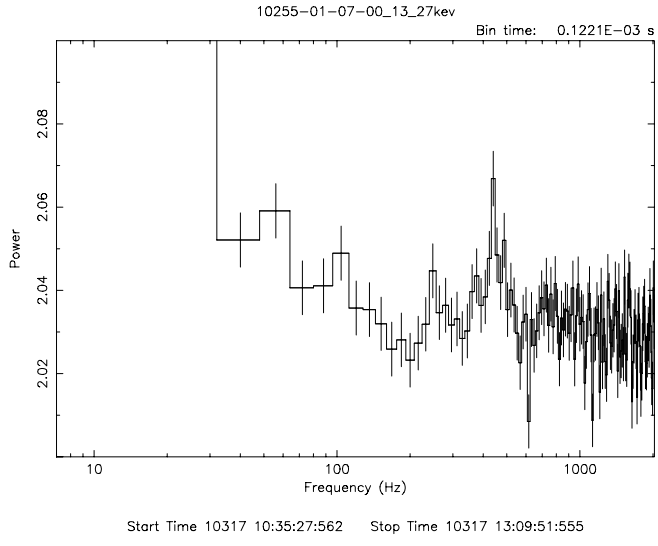

Figure 3.5: RXTE PCA power spectrum computed from the data 22 August 1996 (10255-01-07-00) of GRO J1655-40 in high energy band 13-27 keV

results of Remillard et al. (1999b); 10255-01-06-01 on 16 August 1996, 10255-01-07-00 on 22 August 1996, 10255-01-17-00 on 27 October 1996, 10255-01-04-00 on 1 August 1996 with exposure time 4290 sec. Both 300 Hz and 450 Hz QPOs are detected data sets 10255-01-06-01, 10255-01-07-00, 10255-01-17-00 (Strohmayer 2001). They were all seen in the flaring state. The Figure 3.5 shows the power spectrum which displays twin high frequency QPOs ($\sim$300 Hz and $\sim$450 Hz) in 2-12 keV and 13-27 keV energy band for the observation 10255-01-07-00, respectively. In datasets 10261, 10263, 20187, 90019, 90058, 91404 power spectrums did not show any significant QPOs.

3.4 GRS 1915+105

3.4.1 Introduction

The black hole binary GRS 1915+105 is first discovered galactic source that shows superluminal jet structure (Mirabel & Rodriguez 1994). It was discovered as a X-ray transient by GRANAT/ WATCH (Castro-Tirado 1994). GRS 1915+105 is $\sim 9\pm3$ kpc away from the sun (Chapius & Corbel 2004). Since it is located on the opposite side of the glactic plane, the dust along the line of side makes impossible to examine the source in the optical band of the electromagnetic spectrum (Mirabel et al. 1994; Chaty et al. 1996). Castro-Tirado et al. (1996) proposed that GRS 1915+105 has low mass companion whereas Eikenbery et al.

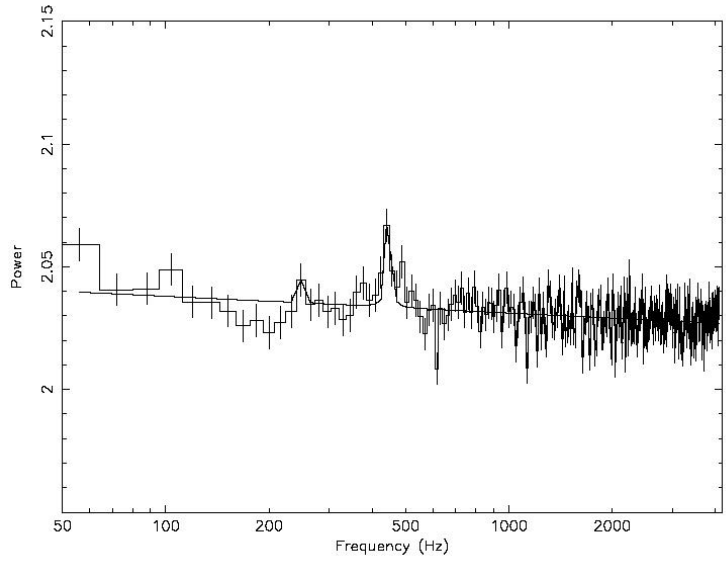

Figure 3.6: RXTE PCA power spectrum computed from the data 22 August 1996 (10255-01-07-00) in high energy band 13-27 keV fitted with Lorentzian and power law model; lines are centered at 250.4 Hz and 446.7 Hz, respectively

(1998b) proposed the emission lines in the infrared band of the spectrum arise in an accretion disk of the high mass (Oe/Be type) companion.

GRS 1915+105 is most luminous hard X-ray source known in the galaxy (Paciesas et al. 1996). The X-ray luminosity in the high state is $\sim 5 \cdot 10^{39}$ergs s^{-1} and in the low state $\sim 10^{38}$ergs s^{-1}. The low mass companion is K type giant with mass $(0.8 \pm 0.5) M_{\odot}$ rotating in 33.5 days so that the accretion takes place via Roche Lobe overflow (Greiner et. al. 2001b; Harlaftis & Greiner 2004; Eikenberry & Bandyopadhyay 2000). The mass function $f(M) = (9.5 \pm 3.0) M_{\odot}$,which is the lower limit to the mass of the compact object using the mass of the donor star and the inclination angle $\theta = 70^{\circ} \pm 0.2^{\circ}$, indicates that the donor star orbits around

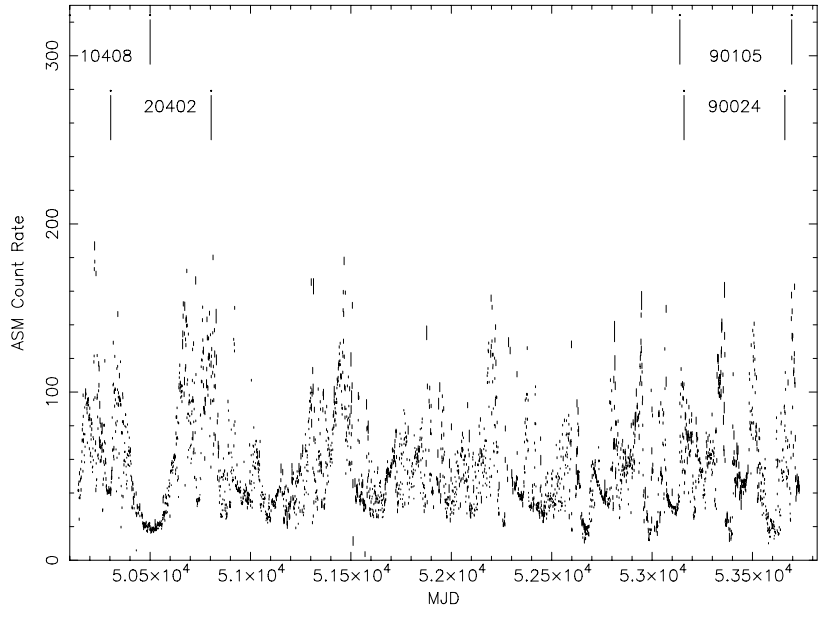

Figure 3.7: RXTE ASM light curve of GRS 1915+105 between 01 January 1996 and 31 December 2005

(14.0 ±4.4) $M_{\odot}$ black hole with an orbital separation of (108±4)$R_{\odot}$ (Harlaftis & Greiner 2004).

Using the rotational velocity of the donor $v \sin i = (26 \pm 3)$km s^{-1} (Harlaftis & Greiner 2004) and synchronous rotation with the orbital period period 33.5 days, Zdzarski et al. (2005) found the donor radius of $R_2 = (17.2 \pm 2.0) \sin^{-1} i R_{\odot}$.

GRS 1915+105 is a X-ray transient source. Two sudden outburst have been

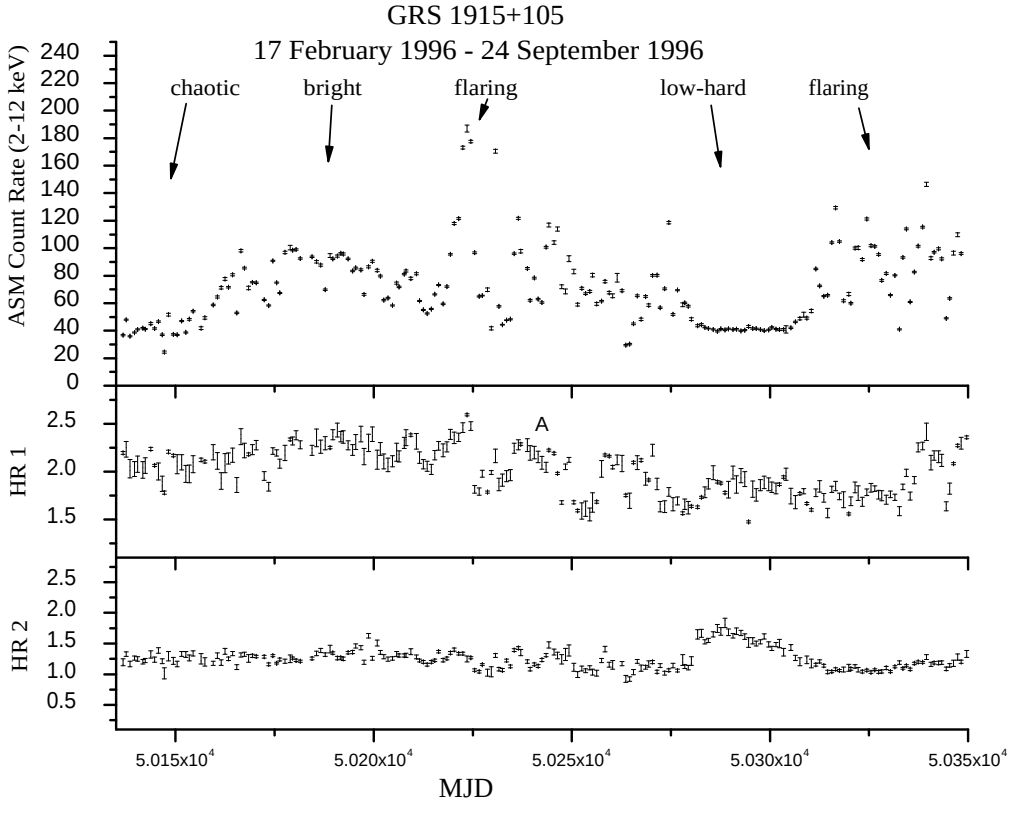

Figure 3.8: RXTE ASM light curve of GRS 1915+105 between 17 February 1996 and 24 September 1996 in the 2-12 keV

observed with BATSE (25-100 keV) from 1992 August until 1993 September (Harmon, Pacesias & Fishman 1992) and from 1993 December until 1994 April. Since 1996 April 6, GRS 1915+105 have been observed with All-Sky Monitor (ASM) on board the Rossi X-Ray Timing Explorer (RXTE) (Bradt, Rothschild & Swank 1993). The radio counterpart was monitored until late 1993. The observed radio spectrum is consistent with radio flares of the persistent source Cyg X-3 and Cir X-1. Between 1996-1998, GRS 1915+105 was observed in radio band with Green

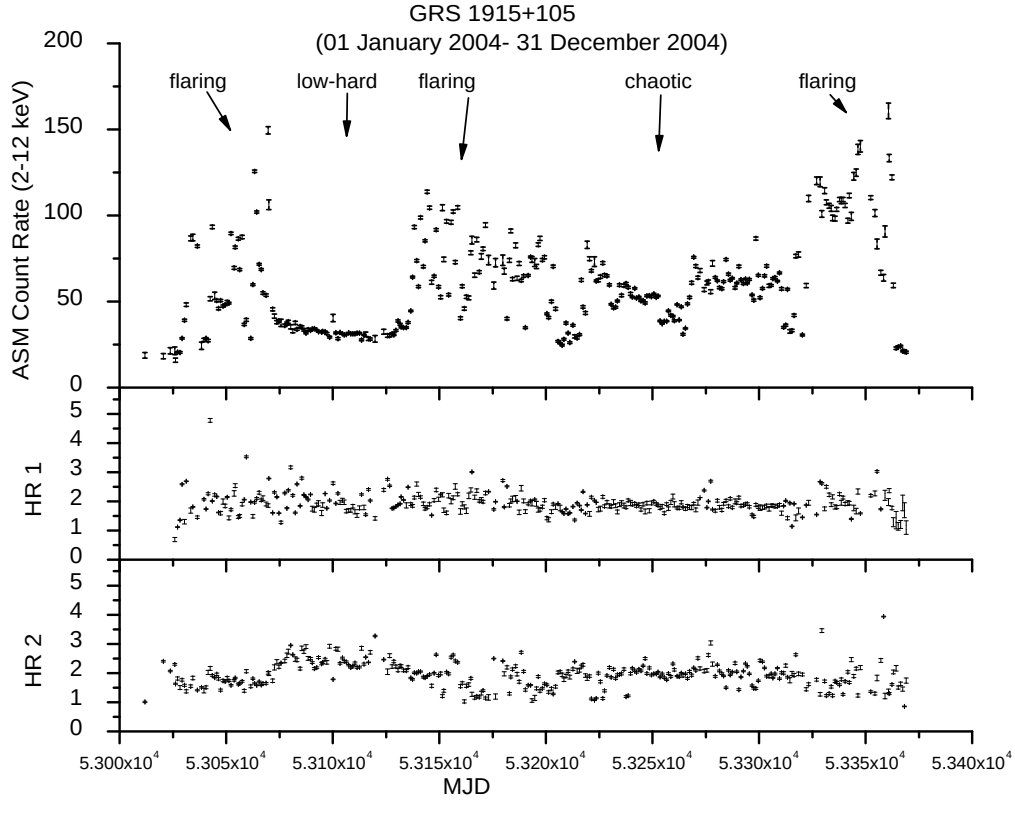

Figure 3.9: RXTE ASM light curve of GRS 1915+105 between 01 January 2004 and 31 December 2004 in the 2-12 keV

Bank Interferometer (GBI), in soft X-ray band with All-Sky Monitor (ASM) on board Rossi X-Ray Timing Explorer (RXTE) and in hard X-ray band with Burst and Transient Source Experiment (BATSE) on board Compton Gamma Ray Observatory (CGRO). The radio and gamma-ray (> 20 keV) correlation was observed on this time interval. Greiner et al. 1996 presented the X-ray variability which includes brightness sputters, large amplitude oscillations, fast oscillations of GRS 1915+105 using RXTE data. Narrow quasi-periodic oscillations were observed in the X-ray band using with Indian X-ray Astronomy Experiment data (Agrawal et al. 1996) and RXTE data (Morgan & Remillard 1996). Chen, Swank & Taam (1997) discovered that the narrow quasi-periodic oscillations are a characteristic of hard X-ray state similar to the other black hole candidates. Morgan, Remillard & Greiner (1997) defined four different X-ray states as chaotic, bright, flaring and low-hard and their QPO characteristics. They revealed 3 mHz to 67 Hz frequency range QPOs based on the power spectra, light curves and energy spectra. But they are not consistent with the other black hole binary X-ray state characteristics. Paul et al. (1998b) discovered that 0.5-10 Hz QPO traces the change of state from a flaring to a low-hard state quite smoothly along with other X-ray characteristics like the low frequency variability (Rao, Yadav & Paul 2000). The X-ray luminosity of GRS 1915+105 ($\sim 2 \times 10^6 L_\odot$) far exceeds the Eddington luminosity limit for a $3M_\odot$ object($10^5 M_\odot$).

The superluminal motions of GRS 1915+105 was discovered with the satellite GRANAT (Mirabel & Rodriguez 1994). The extensive X-ray and infrared observations showed that there is a correlation between the hard X-ray emission from

the accretion disk with the non-thermal infrared emission coming originated from jet production (Eikenberry et al. 1998).

3.4.2 ASM Observations of GRS 1915+105

The ASM light curve of GRS 1915+105 between 50000 (10 October 1995) and 53530 (09 June 2005) in Modified Julian Date (MJD) are seen in the Figure 3.7. The appearance of the hardness ratios and ASM light curves suggests

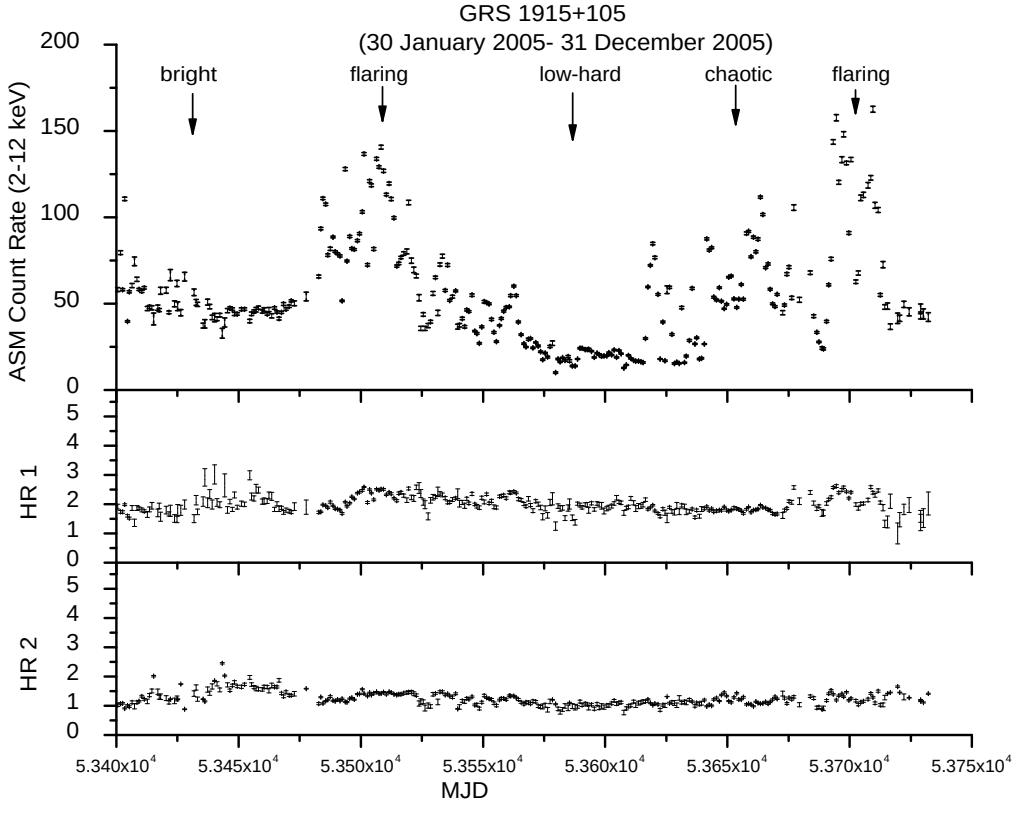

Figure 3.10: RXTE ASM light curve of GRS 1915+105 between 30 January 2005 and 31 December 2005 in the 2-12 keV

that GRS 1915+105 displays four X-ray states. Between MJD 50000 and 53530 ASM light curves are incredibly variable. Morgan et al. (1997) suggest that the source migrate through four states; "chaotic", "bright", "flaring" and "low-hard". Before MJD 50170 (28 March 1996) the source was seen in its chaotic state which observed highly variable. The flux is about 0.66 ± 0.24 Crab at 2-12 kev while HR1 (1.90)and HR2 (1.32) values indicates that soft X-ray spectrum is applicable. During the interval MJD 50170 and 50220 (17 May 1996) the source appeared to be in its steady bright state with hardness-ratio values HR1 (2.18), HR2 (1.39) and the average ASM X-ray flux 1.1 Crab (2-12 kev). During the interval 50220 and 50280 (16 July 1996), the source was in its flaring state with hardness ratios HR1=2.08 and HR2=1.31 but very high ASM X-ray flux. Between the 50280 and 50310 (15 August 1996) the source evolved to low state with average flux 0.51±0.002 Crab and hardness ratios (1.82,1.74)(Morgan, Remillard, Greiner 1997)(see Figure 3.8).

After 50310 the source appeared to return flaring state again. During the time intervals between 50310 and 53005 (01 January 2004) GRS 1915+105 showed many flaring activity and between 53005 and 53080 (16 March 2004) the source seemed to be in its flaring state as shown in the Figure 3.9. Using WebPIMMS in this time interval we calculated the X-ray flux which was about $\sim 1.880 \times 10^{-8}$ergs cm^{-2}s^{-1} with unabsorbed flux of $\sim 3.168 \times 10^{-8}$ergscm^{-2}s^{-1} in (2.0-12.0 keV) corresponding ASM count rate about 50 cps. Between 53070 and 53140 (06 March 2004) the source was appeared to be in its low-hard state with unabsorbed flux $\sim 2.113 \times 10^{-8}$ergs cm^{-2}s^{-1}. Between 53140 and 53210 (24

July 2004) GRS 1915+105 evolving through flaring state with unabsorbed flux $\sim 3.294 \times 10^{-8}$ergs cm^{2}s^{-1}. Between 53210 and 53270 (22 September 2004) the source was in its bright state with unabsorbed flux $\sim 1.934 \times 10^{-8}$ergs cm^{-2}s^{-1}. GRS 1915+105 was evolving through chaotic state between 53270 and 53320 (11 November 2004) and corresponding unabsorbed X-ray flux in 2-12 keV was $\sim 2.321 \times 10^{-8}$ergs cm^{-2}s^{-1}. But through 53352 (13 December 2004) the X-ray flux rose and reached to 3.094×10^{-8}ergs cm^{-2}s^{-1}.

During 2005, GRS 1915+105 displayed highly variable flaring activity shown in the Figure 3.10. Between MJD 53400 (30 January 2005) and 53480 (20

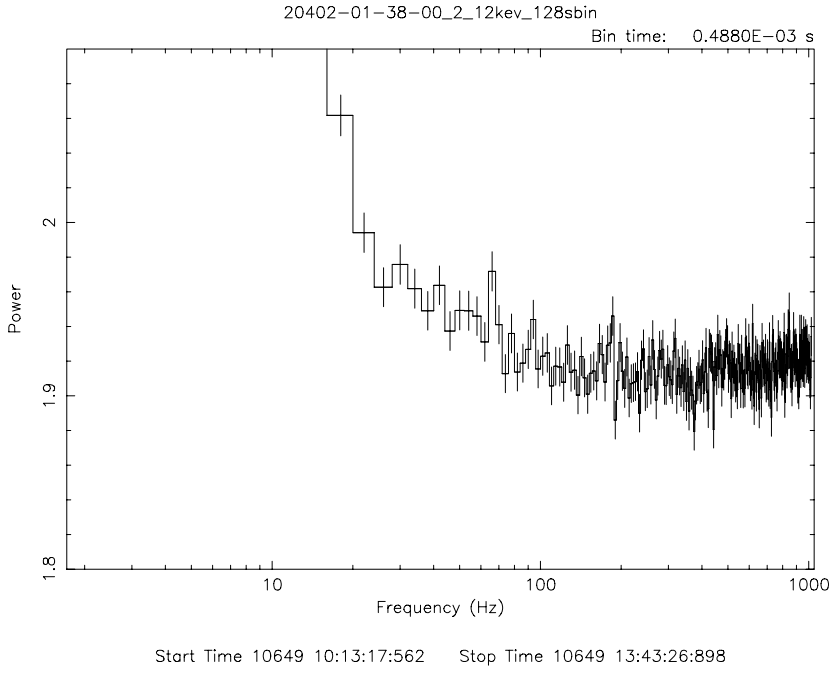

Figure 3.11: RXTE PCA power spectrum computed from the data 20 July 1997 (20402-01-39-02) of GRS 1915+105 in low energy band 2-12 keV

April 2005) it migrated to bright state once more time and corresponding unabsorbed X-ray flux was $\sim 1.88 \times 10^{-8}$ergs cm^{-2}s^{-1} in 2-12 keV. Through MJD 53560 (09 July 2005) the source was evolving its flaring state with $\sim 2.493 \times 10^{-8}$ergs cm^{-2}s^{-1} unabsorbed X-ray flux. The low-hard state characteristics was seen one more time with low ASM count rate between MJD 53560 and 53610 (28 August 2005) whose unabsorbed flux was $\sim 8.822 \times 10^{-9}$ergs cm^{-2}s^{-1}. The chaotic state dominated between the time interval 53610 and 53690 (16 November 2005) with X-ray flux $\sim 1.649 \times 10^{-8}$ergs cm^{-2}s^{-1}. At the end of the year 2005 the source appeared to be in its final flaring state with very high flux ($\sim 3.069 \times 10^{-8}$ergs cm^{-2}s^{-1}).

3.4.3 PCA Power Spectra of GRS 1915+105

We began to analyze RXTE/PCA A01, AO2, AO9 public data retrieved from HEASARC browser web site. The data set which we began to investigate the QPO feature in Proposal ID 10428 under AO1 dataset with a number of 31 RXTE pointed observations, 20402 under AO2 observation set with a number of 97 RXTE pointed observations, 90105 and 90024 under AO9 observations with a number of 22 and 2 RXTE pointed observations, respectively. We analyzed 122 total observations for GRS 1915+105 in this thesis (see Table 3.5).

The dataset with observation ID 10428 consist of $62\mu s$ single bit mode data covering energies smaller than 13 keV and $62\mu s$ event mode data covering energies greater than 13 keV. The data under Proposal 20402 includes $62\mu s$ event mode data recording events greater than 13 keV and $125\mu s$ resolution single bit mode

Table 3.5: Observation date and ID List of galactic microquasar GRS 1915+105

Start Date day/month/year	End Date day/month/year	XTE Obs ID	PI Name	# of Obs.
09/04/1996	29/10/1996	10408	TOO	31
07/11/1996	22/11/1997	20402	TOO	97
03/07/2004	18/10/2005	90024	Morgan	2
13/05/2004	21/11/2005	90105	Rodriguez	22

data recording events under energies 13 keV. The dataset with proposal ID 90024 made up $500\mu s$ resolution event mode data including 13 keV and higher energies and 90105 with $500\mu s$ resolution event mode data for higher energies and $125\mu s$ resolution single bit mode data for lower energies than 13 keV.

We first began investigating the QPO feature in the dataset with Proposal ID 10408. We computed 31 power spectra for each observation separately for both low energy band (2-12 keV) and hard band (13-27 keV). We used 64s and 32s, 64s, 128s intervals spanning the range from 0.250 to 512 Hz. Beside $\sim$67 Hz QPO $\sim$40 Hz was also detected in the datasets covering the energies 13-27 keV (see Figure 3.11 and 3.12) (Strohmayer 2001). The $\sim$40 Hz QPOs whose significance level is greater than 3σ, 4σ and more than 5σ are listed in the Table 3.6. We did not detect 67 Hz QPO in low energy band. We also analyzed the archive data with Proposal ID 20402. Even both of them were seen simultaneously in the

Table 3.6: Significance Levels of 40 Hz QPOs found in microquasar GRS 1915+105

Date of Observation day/month/year	XTE Obs ID	Confidence Limits	Corresponding X-ray State
17/11/1997	20402-01-55-00	More than 3σ (2-12 keV)	flaring
15/05/2004	90105-01-03-00	More than 4 σ (2-12 keV)	flaring
19/10/2004	90105-03-03-02	More than 5 σ (2-12 keV)	chaotic

Table 3.7: Significance Levels of 67 Hz QPOs found in microquasar GRS 1915+105

Date of Observation day/month/year	XTE Obs ID	Confidence Level	Corresponding X-ray State
05/05/1996	10408-01-06-00	More than 5σ (13-27 keV)	bright
25/07/1997	20402-01-39-00	More than 5σ (13-27 keV)	flaring
29/07/1997	20402-01-39-02	More than 5σ (13-27 keV)	flaring
17/11/1997	20402-01-55-00	More than 4σ (13-27 keV)	flaring
19/10/2004	90105-03-03-00	More than 3 σ (13-27 keV)	chaotic
18/10/2004	90105-03-02-03	More than 3 σ (13-27 keV)	chaotic
19/10/2004	90105-03-03-02	More than 5 σ (13-27 keV)	chaotic

same power spectrums (20402-01-39-00, 20402-01-39-02, 20402-01-55-00) over 97 power spectrums (Morgan et al. 1997). The 67 Hz QPOs and their significance levels is seen Table 3.7 (Morgan et al. 1997, Strohmayer et al. 2001). Table

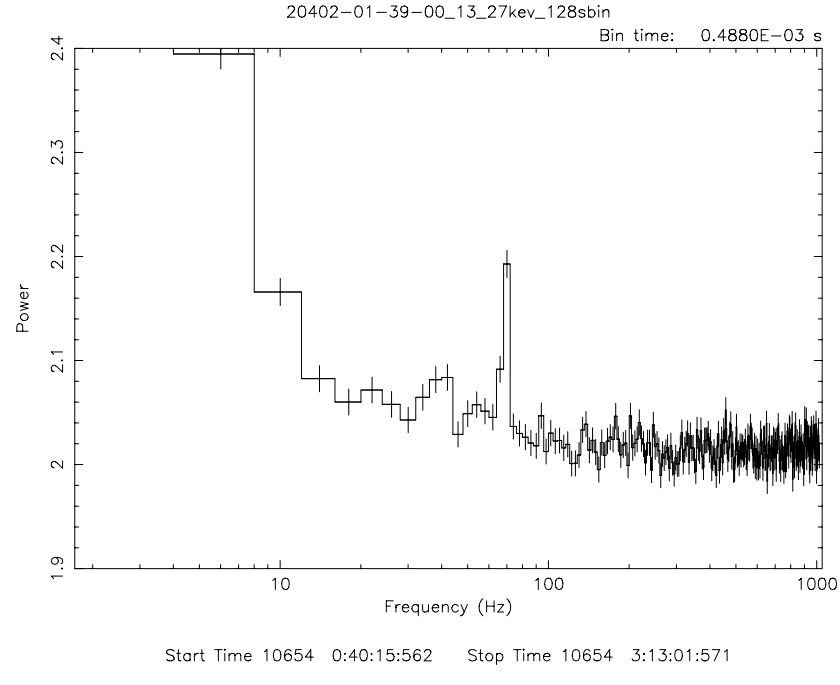

Figure 3.12: RXTE PCA power spectrum computed from the data 20 July 1997 (20402-01-38-00) of GRS 1915+105 in high energy band 13-27 keV

Table 3.8: Significance Levels of 40 Hz and 67 Hz QPOs found in microquasar GRS 1915+105 below 3σ

Date of Observation day/month/year	XTE Obs ID	Confidence Limits	Corresponding X-ray State
20/07/1997	20402-01-38-00	More than 2 σ (13-27 keV)	flaring
20/071997	20402-01-38-00	More than 2 σ (2-12 keV)	flaring
25/07/1997	20402-01-39-00	More than 2 σ (2-12 keV)	flaring
29/07/1997	20402-01-39-02	More than 2σ (2-12 keV)	flaring
22/11/1997	20402-01-56-00	More than 2 σ (2-12 keV)	flaring
19/10/2004	90105-03-03-00	More than 2 σ (2-12 keV)	chaotic
14/05/2005	90105-05-03-01	More than 2 σ (2-12 keV)	flaring
15/05/2005	90105-05-03-05	More than 2 σ (2-12 keV)	flaring
15/05/2004	90105-01-03-00	More than 2 σ (13-27 keV)	flaring
19/10/2004	90105-03-03-00	More than 2 σ (2-12 keV)	chaotic
19/10/2004	90105-03-03-00	More than 2 σ (13-27 keV)	chaotic

3.8 shows QPOs more than 2σ in both hard band and low band. In the other datasets we did not find any significant peak.

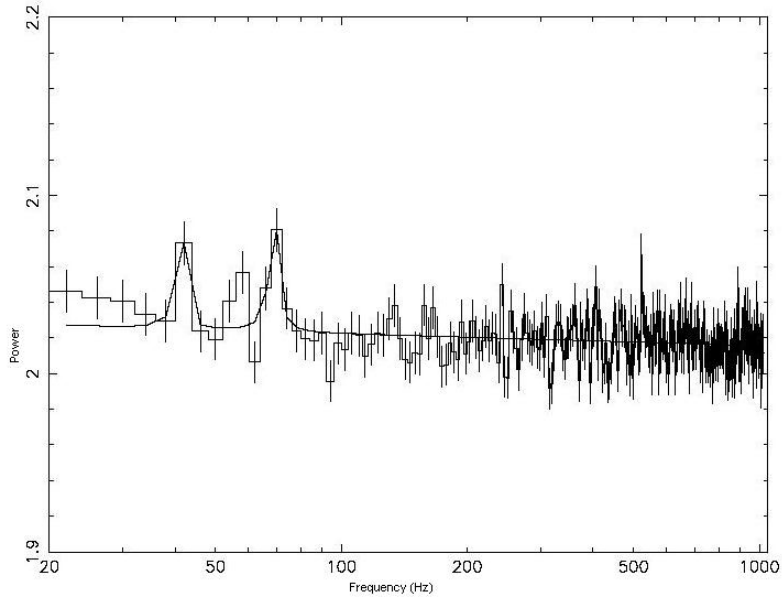

Figure 3.13: RXTE PCA power spectrum computed from the data 20 July 1997 (20402-01-38-00) of GRS 1915+105 in high energy band 13-27 keV fitted with Lorentzian and power law model; lines are centered at 40.96 Hz and 68.69 Hz, respectively

To investigate whether the significant QPO features appear throughout 2004 and 2005 years, we also examined 2 RXTE pointed observation in dataset 90024 and 22 observations in dataset 90105. Some of the 122 computed power spectrums displays $\sim$40 Hz and $\sim$67 Hz. Table 3.6 and Table 3.7 shows the significant QPOs above the level more than 3σ, 4σ and more than 5σ. During 2004-2005 outbursts we did not detect high frequency QPOs simultaneously. The significance levels are calculated with the same way as in GRO J1655-40. We modelled the power spectrum with Lorentzian and power law model to compute the significance limits which is shown in Figure 3.13. We have observed that both high frequency QPOs were seen during soft states; chaotic, bright and flaring as in the case of GRO J1655-40.

CHAPTER 4

CHANDRA AND RXTE JOINT SPECTROSCOPY OF GRS 1915+105

4.1 Introduction

X-ray spectroscopy is key feature of the understanding the physical properties of GRS 1915+105 environment and the behavior of the central black hole. Based on ASCA observations of GRS 1915+105 in 1994-1995, the resonant absorption lines of Ca XX Kα and Fe (XXV, XXVI) Kα and absorption lines of Ni XXVII Kα + Fe XXV Kβ and Ni XXVIII Kα + Fe XXVI Kβ were identified (Kotani et al. 2000). However ASCA is not capable of examining the detailed absorption and emission line components. The High resolution of the High-Energy Transmission Grating (HETG) on board Chandra X-ray Observatory, recent observations of the source with HETG provide more details in extend.

Chandra was launched in 23 July 1999 under "flagship mission" of NASA. Chandra X-ray Observatory consists of four instruments to capture and probe the X-rays from astronomical sources. The incoming X-rays are focused on focal plane instruments; Advanced Charged Coupled Device Imaging Spectrometer (ACIS) and High Resolution Camera (HRC). HRC is used at the focus of Chandra. It detects arrays reflected from the assembly of eight mirrors and allows us

to predict the position of the original X-ray to be determined with high precision. ACIS is the second of the focal plane instruments. It is an array of charge coupled devices (CCDs) and incorporates the CCDs as photon counting X-ray detectors. There are two instruments for the usage of high resolution spectroscopy; High Energy Transmission Grating Spectrometer (HETG) and Low Energy Transmission Grating Spectrometer (LETG). The LETG is a gold grating made of fine wires or bars. The LETG gratings are capable of covering energy range of 0.08 to 2 kev. The detailed spectra made up with LETG in corresponding energy range enable us to measure the temperature, ionization and chemical abundance in the explored region. The HETG was inserted into the optical path behind Chandra's mirror and consist of 336 gold grating facets. The HETGS has two different grating types that disperse into two independent spectra. The medium energy gratings (MEGs) have an energy range of about 0.4-5 keV, depending on the observation parameters, and the high energy gratings (HEGs) have an energy range of about 0.8 to 10 keV. The HETG intercepts the X-rays reflected back from the mirrors and changes their direction. ACIS or HRC detects the location and allow us to determine the X-ray's energy.

In this chapter we present the spectral features of the time-averaged X-ray spectrum of GRS 1915+105 obtained with the high resolution gratings (HETG) on board Chandra and Proportional Counter Array (PCA) on board RXTE .

Table 4.1: RXTE Proportional Counter Array Spectrum Parameters of GRS 1915+105

Parameter	Case 1	Case 2
$N_H(10^{22}\mathrm{cm}^{-2})$	9.23±1.20	6.89±0.09
Iron-line energy (keV)	6.78±0.06	6.17±0.02
Iron-line σ (keV)	0.60±0.07	1.04±0.10
Iron-line normalization (photons $\mathrm{cm}^{-2}\mathrm{s}^{-1}$)	0.01±0.01	0.04±0.01
Power-law index	2.40±1.69	2.44±0.09
Power-law Normalization (photons $\mathrm{keV}^{-1}\mathrm{cm}^{-1}\mathrm{s}^{-1}$)	8.99±7.59	7.18±0.31
Disk Blackbody kT (keV)	2.17±0.72	4.83±0.11
Disk Blackbody Normalization $[\mathrm{km}^2(10\mathrm{kpc})^{-2}]$	0.80±52.38	0.26±0.03
Reduced χ^2	1.38(32 d.o.f.)	0.27(35 d.o.f.)

4.2 RXTE-PCA Spectrum Analysis

We observed GRS 1915+105 in flaring (06 March 2004). To have a better spectral coverage we also analyzed RXTE PCA observations of 07 March 2004 (MJD 53071) part of which simultaneous to Chandra data with exposure time 30.14 ksec of 06 March 2004 of GRS 1915+105. In this chapter we aimed to observe the spectral properties of flaring state and compare our results with previous results which were mentioned before.

The PCA spectrum was analyzed with XSPEC 11.3 software. In 3-20 keV energy range, systematic errors of 2 % were used in fitting data. The best fit to the continuum model is a disk blackbody plus a power-law component that describes the RXTE data.

We modelled the spectra with powerlaw (Morrison & McCammon 1983) with Comptonization of soft X-ray seed photons, assumed here to be a disc blackbody with a maximum temperature, T_{in} (Mitsuda et al. 1984) and iron line at ~ 6.78 keV. The DISKBB model previously used by Lee et al. (2002). In Case 1 we set the maximum inner disk temperature of the disk ~ 2 keV to get more physical

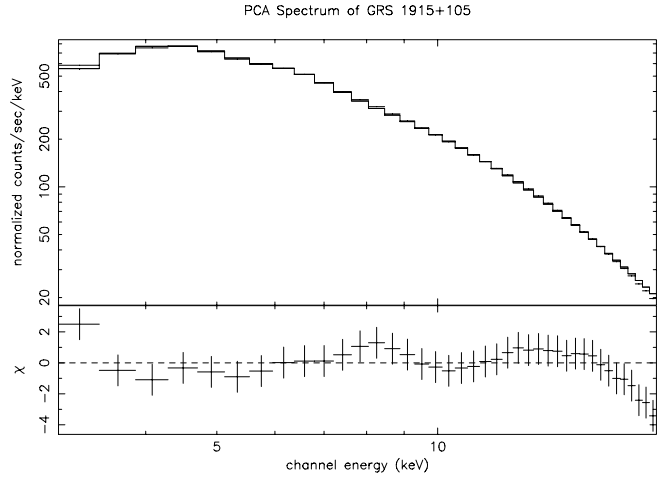

Figure 4.1: RXTE continuum of GRS 1915+105 based on Chandra continuum model overplotted on RXTE PCA data (Case 1)

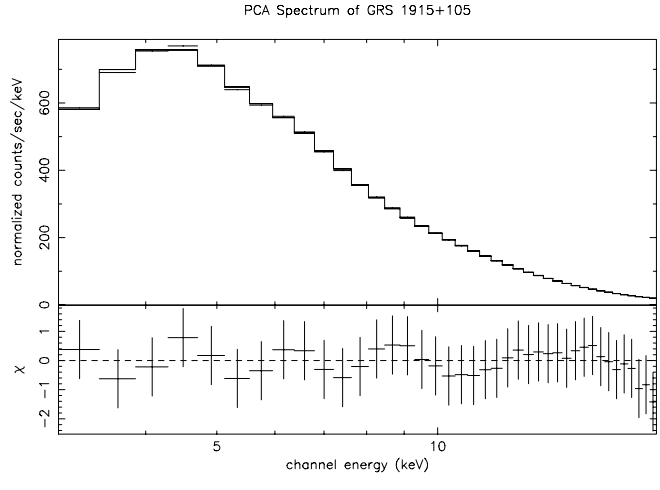

Figure 4.2: RXTE continuum of GRS 1915+105 based on Chandra continuum model overplotted on RXTE PCA data (Case 2)

results. In Case 2, we do not freeze kT_{in} to observe the changes in parameters. Best fit parameters are described in the Table 6.1. Using the Case 1 the 3-20 keV flux is found to be 9.4746×10^{-9} ergs $cm^{-2}s^{-1}$. The resulting inner disk temperature which is found in Case 2 is very high ($kT_{disk} > 3keV$) which has already discussed by Muno et al. (1999, 2001) and Fuchs et al. (2003). They obtained that result while fitting the powerlaw model plus disk blackbody and gaussian low-hard state of GRS 1915+105. Zdziarski et al. (2001) suggest that high temperature may indicate either invalidness of diskbb model or the different emission mechanism which may due to comptonisation of thermal plasma. The specific characteristic of hard state black hole binaries is high-energy cutoff at $\geq$ 100 keV which is due to the effects of Compton recoil and gravitational redshift close to the black hole horizon (Laurent & Titarchuk 1999, Zdziarski et al. 2001). Since we modelled the data up to energies 20 keV, we do not observe high energy cutoff at $\geq$ 100 keV.

4.3 Chandra HETG Spectrum Analysis

We extracted the first order dispersed spectra (m = $\pm$1 for HEG and MEG) for a total of four spectra since the spectral bandpass and efficiency reduce as the order rises. We merged four HEG (m= $\pm$ 1) and MEG (m= $\pm$ 1) spectra into two combined spectra in order to increase the signal to noise ratio. For the fit, we binned data to obtain a minimum 16 counts per bin for both HEG and MEG spectra. We reduced data using the CIAO 3.2 software package and CALDB 3.3.0.1.

Table 4.2: Chandra HEG ($m = \pm 1$) and MEG ($m = \pm 1$) Case 1 Spectrum Parameters of GRS 1915+105

Parameter	HEG	MEG
$N_H(10^{22}\mathrm{cm}^{-2})$	4.18±0.13	4.18±0.13
Iron-line energy (keV)	6.56 ±0.06	6.56 ±0.06
Iron-line σ (keV)	0.19±2.09	0.19±2.09
Iron-line normalization (photons $\mathrm{cm}^{-2}\mathrm{s}^{-1}$)	0.01±0.01	0.01±0.01
Power-law index	1.93±0.24	2.14±0.13
Power-law Normalization (photons $\mathrm{keV}^{-1}\mathrm{cm}^{-1}\mathrm{s}^{-1}$)	2.46±0.30	1.48±0.20
Disk Blackbody kT (keV)	4.34±0.16	4.34±0.16
Disk Blackbody Normalization $[\mathrm{km}^2(10\mathrm{kpc})^{-2}]$	1.75±0.31	2.72 ±1.09
Reduced χ^2	2.53 (385 d.o.f.)	

The first order HEG and MEG spectra of GRS 1915+105 are shown in the Figure 6.2 and Figure 6.3. We modelled the spectra in terms of Comptonization of soft X-ray seed photons, assumed here to be a disc blackbody with a maximum temperature, T_{in} and powerlaw plus iron line at ~ 6.57 for Case 1 and ~ 6.49 for Case 2. The best fit parameters are also shown in Table 6.2 and Figure 6.3.

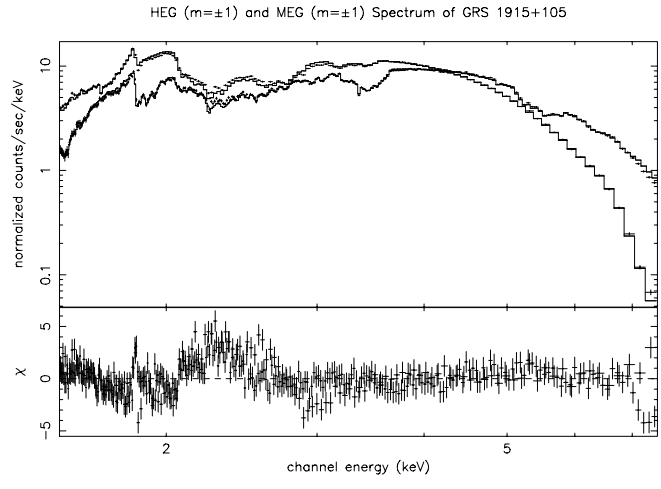

Figure 4.3: Case 1 Chandra HETG continuum of GRS 1915+105 over plotted on Chandra HEG (order m=± 1 combined, lower curve) and MEG (order m=± 1 combined, upper curve)

Table 4.3: Chandra HEG ($m = \pm 1$) and MEG ($m = \pm 1$) Case 2 Spectrum Parameters of GRS 1915+105

Parameter	HEG	MEG
$N_H(10^{22}\mathrm{cm}^{-2})$	3.82± 0.04	3.82± 0.04
Iron-line energy (keV)	6.48 ±0.13	6.48 ±0.13
Iron-line σ (keV)	0.23± 2.45	0.23± 2.45
Iron-line normalization (photons $\mathrm{cm}^{-2}\mathrm{s}^{-1}$)	0.01±0.01	0.01±0.01
Power-law index	1.2 ±0.74	0.80±0.07
Power-law Normalization (photons $\mathrm{keV}^{-1}\mathrm{cm}^{-1}\mathrm{s}^{-1}$)	1.15±0.43	0.60 ±0.12
Disk Blackbody kT (keV)	1.60±0.06	1.60±0.06
Disk Blackbody Normalization $[\mathrm{km}^2(10\mathrm{kpc})^{-2}]$	33.56 ±255.04	37.30±83.13
Reduced χ^2	2.63 (384 d.o.f.)	

In Case 1 disk temperature is high ($kT_{disk} > 3keV$) as we have found at PCA parameters while in Case 2 the disk temperature is in reasonable range. The absolute flux calculated in Case 2 is relatively low 7.76×10^{-9} ergs $\mathrm{cm}^{-2}\mathrm{s}^{-1}$. All parameter ranges are quoted for reduced χ^2 =2.53. The reduced χ^2 calculated in Chandra HEG and MEG instrument is worse than PCA reduced χ^2. Spectrum indicates complexity in the absorption and emission lines. ASCA and Chandra spectral data identified in this source absorption lines of Ca XX K α, Fe (XXVI, XXVI) K α and Ni XXVII α+ Fe XXV K β Ni XXVIII K α+ Fe XXVI Kβ as well as neutral Fe Kα and ionized Fe XXV emission edges, neutral photoelectric K edges Fe K (7.12 keV), Mg K (1.38 keV), Si K (1.84 keV), S K (2.47 keV) (Lee et al. 2002). Since we do not fit those edges, rise of reduced χ^2 is reasonable.

The spectra is well fitted to the model consisting of a power law due to comptonisation of photons in hot corona with disk blackbody and gaussian line centered at $\sim$ 6.5 keV. The power law index which we found measured in PCA-HETG joint spectrum (see Figure 6.5)is relatively hard ($\Gamma > 3.7$) on 07 March 2004. It may indicate that the source is in hard-state. ASM light curve in MJD 53071 (07 March 2004) predicts that the source made transition from bright state to low

hard state. Fuchs et al. (2003) suggested the 3-20 keV energy range power law index was $\Gamma = 2.94 \pm 0.01$ in PCA+ HEXTE joint spectrum. Fender et al. (1999), Rau & Greiner (2003) discussed the power law origin of spectra. The highenergy disk emission of GRS 1915+105 on 07 March 2004 is consistent with the low-hard state of the source with power law dominated spectrum ($\Gamma \sim 2.4$) (McClintock & Remillard 2004). The high disk temperature origins hot gas structure in disk wind or disk atmosphere that mostly absent from most of the black hole accretion models. Furthermore Lee et al. (2002) suggested that absorption features point to hot disk atmosphere or disk wind origin. We have faced with high temperature in HETG, PCA and HETG and PCA co-added spectra. The correlation of hard state with persistent radio emission of GRS 1915+105, reader is directed

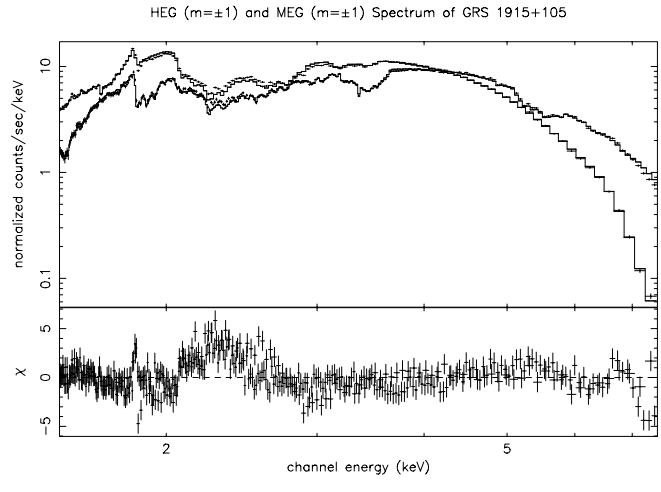

Figure 4.4: Case 2 Chandra HETG continuum of GRS 1915+105 over plotted on Chandra HEG (order m=± 1 combined, lower curve) and MEG (order m=± 1 combined, upper curve)

Table 4.4: Fit Parameters of Simultaneous PCA- HETG Spectra from GRS 1915+105

Parameter	HEG	MEG	PCA
$N_H(10^{22}\mathrm{cm}^{-2})$	4.34± 0.05	4.34 ± 0.06	4.34±0.05
Iron-line energy (keV)	6.54 ±0.05	6.54 ±0.05	6.55± 0.01
Iron-line σ (keV)	0.24± 2.45	0.24± 2.46	0.02±0.01
Iron-line normalization (photons $\mathrm{cm}^{-2}\mathrm{s}^{-1}$)	0.30±0.23	0.01±0.01	0.01±0.01
Power-law index	2.20 ±0.01	2.20± 0.01	2.20± 0.01
Power-law Normalization (photons $\mathrm{keV}^{-1}\mathrm{cm}^{-1}\mathrm{s}^{-1}$)	2.82±0.13	1.73±0.11	3.67±0.08
Disk Blackbody kT (keV)	3.47±0.01	3.47±0.01	3.47±0.01
Disk Blackbody Normalization $[\mathrm{km}^2(10\mathrm{kpc})^{-2}]$	4.38 ±0.34	5.34±0.33	1.34±0.09
Reduced χ^2	2.49 (420 d.o.f.)		

to Fuch et al. (2003), Rao & Wadavale (2001). To produce the Fe emission line at ~ 6.5 keV, the accretion disc must efficiently reflect primary photons, even at the innermost radii. Done et al. (2004) also confirm the presence of cold disc reflection in the X-ray spectra of GRS 1915+105, and fit the residuals at ~ 6.4 keV with broad and relativistic line models. The broad iron line is produced by iron in the and width is caused by the high velocity material in the disk.

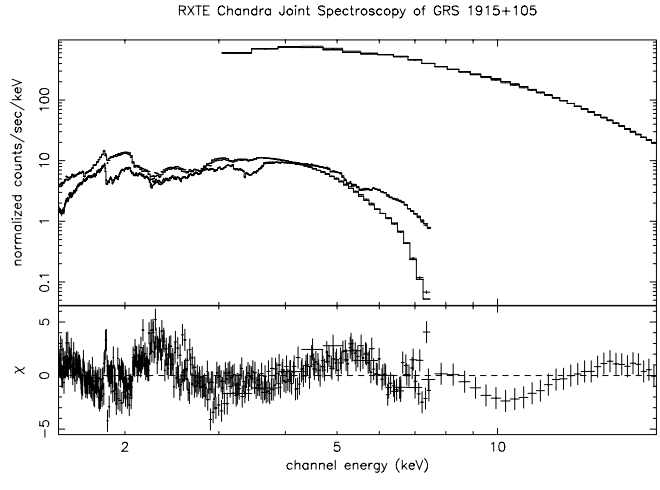

Figure 4.5: Fits to simultaneous PCA- HETG spectra from GRS 1915+105

CHAPTER 5

CONCLUSION AND DISCUSSION

In this thesis RXTE and Chandra observations of galactic microquasars GRO J1655-40 and GRS 1915+105 were presented. Using RXTE pointed observations of GRO J1655-40 and GRS 1915+105, we studied high frequency QPOs which were observed before by Strohmayer (2001). We examined totally 99 RXTE pointed observations for GRO J1655-40 spanning 9 years between 1996 and 2005 covering 1996 and 2004 outbursts. Throughout 9 years four canonical X-ray states are seen in the ASM light curves of the source. We presented corresponding X-ray flux of each canonical states. The twin high frequency QPOs ($\sim$300 Hz and $\sim$ 450 Hz) were seen during only in flaring state. Strohmayer (2001) and Remillard et al. (1999b) previously found both high frequency QPOs; $\sim$ 300 Hz in low energy band (2-12 keV) and $\sim$450 Hz in high energy band (13-27 keV). These two high frequency QPOs sometimes appeared simultaneously. We did not detect any extra twin high frequency QPOs in this time interval above 3σ confidence level but we observed both $\sim$ 300 Hz and $\sim$ 450 Hz QPOs during 1996-1997 outbursts which were previously seen by Strohmayer (2001). We investigated totaly 122 RXTE pointed observations for GRS 1915+105 spanning almost 2 years covering 1996-1997 and 2004-2005 outbursts. We also searched for $\sim$40 Hz

in low energy band (2-12 keV) and ∼67 Hz QPOs in high energy band (13-27 keV) among 122 datasets covering 1996-1997 and 2004-2005 outbursts of GRS 1915+105. Four canonical X-ray states were observed and their corresponding flux's are calculated for the source. We detected both ∼40 Hz and ∼67 Hz QPOs which were previously reported by Morgan et al. (1997) and Strohmayer (2001). These two high frequency QPOs were also sometimes seen simultaneously and observed as a characteristic of soft states (chaotic,bright and flaring)(Strohmayer, 2001). No extra QPOs found in 1996-1997 and 2004-2005 outbursts of GRS 1915+105 above 3σ confidence level. In the Chandra and RXTE joint spectra chapter, we aimed to determine the spectral properties of flaring state seen in GRS 1915+105 using 07 March 2004 RXTE pointed data part of which simultaneous to Chandra pointed data with exposure time 30.14 ksec of 06 March 2004. Diskbb, Powerlaw and cold absorption absorber was found to be appropriate spectral models. We found very high inner disk temperature (kT$>$ 3 keV) which were previously discussed by Zdziarski et al. (2001), Monu et al. (1999, 2001) and Fuchs et al. (2003). We found the powerlaw photon index in the range of ∼1.9-2.4.

There has been recent models which were aimed to explain the origin of high frequency QPOs and their implications on neutron stars and black holes. After the detection of a pair of high frequency QPOs in black hole binaries GRO J1655-40 and GRS 1915+105, it is reasonable that the other black hole binaries may display a pair of high frequency QPOs as well. Those observed high frequency oscillations may reveal different physical mechanisms and also has implications

on black hole spin. Indeed the kilohertz twin QPO mechanisms in neutron star systems may be analogous to the high frequency QPOs seen in black hole binary systems in terms of their similarities in their hard energy spectra high coherence, relative frequency spacing (Strohmayer 2001). But not all the models applied on kilohertz QPOs in neutron star systems are applicable to the black hole binary QPOs because of the lack of solid surface, for example, the sonic point beat-frequency model of Miller, Lamb & Psaltis (1998).

If a black hole's orbital frequency of innermost stable orbit (ISCO) is greater

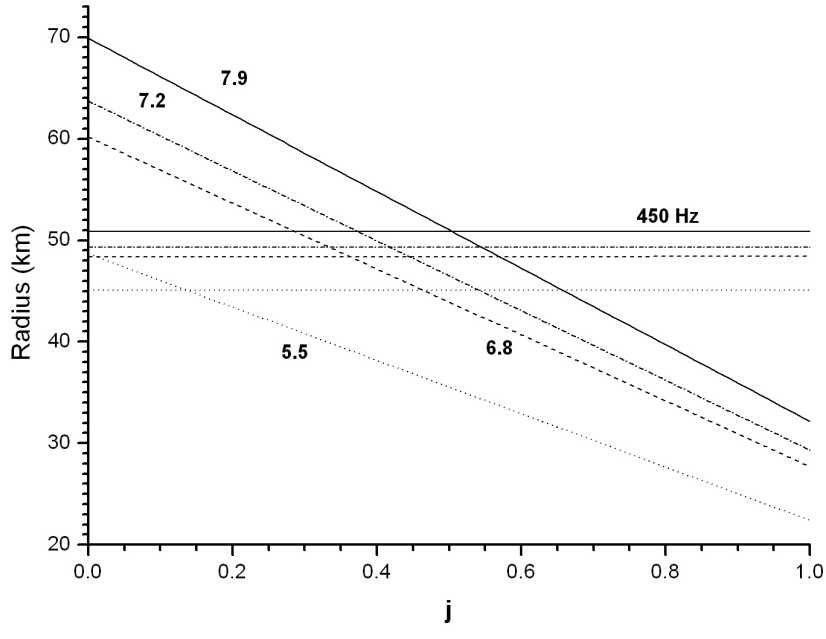

Figure 5.1: Radius of ISCO as a function of dimensionless black hole angular momentum j for the mass limits for GRO J1655-40 of Shahbaz et al. (1999) and Orosz & Bailyn (1997). The ISCO radius is calculated for different masses (5.5, 6.8, 7.2, 7.9 $M_{\odot}$) and denoted as curves. 450 Hz orbital frequency and its corresponding radii and masses are also shown in the figure.

than or equal to 450 Hz then the black hole mass must be between 5.9 and 7.9 $M_{\odot}$ with non-zero angular momentum (Shahbaz et al. 1999). In Figure 6.1 and we have plotted that ISCO radius as a function of dimensionless angular momentum j for different mass limits of GRO J1655-40 (Orozs & Bailyn et al. 1997). Using the definition of radius of the innermost stable orbit in first order j;

$$r_{ISCO} \approx (\frac{6GM}{c^2})(1 - 0.54j) \tag{5.1}$$

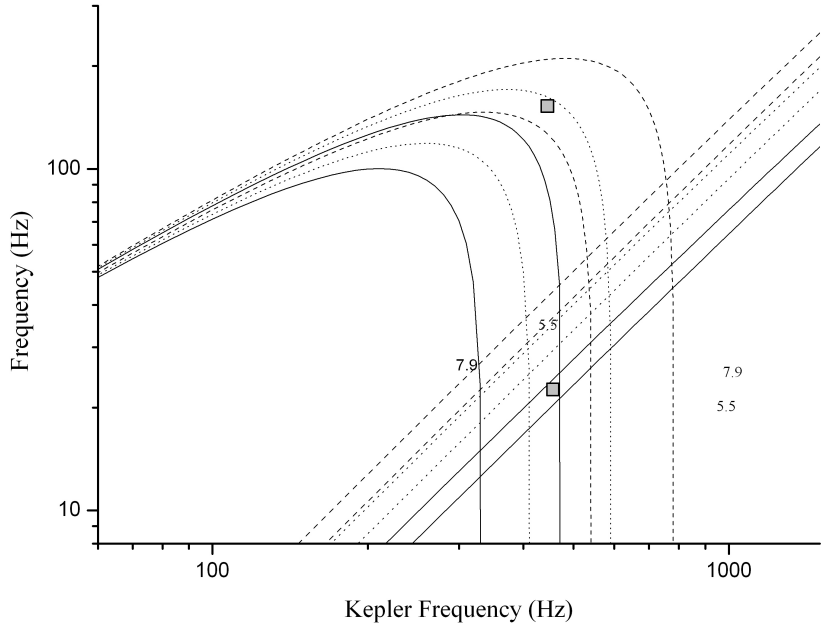

Figure 5.2: Radial epicyclic frequency (curved lines) and the nodal frequency (diagonal lines) versus Keplerian frequency for mass limits $5.5M_{\odot} \leq M \leq 7.9M_{\odot}$ for GRO J1655-40 and for different values of dimensionless angular momentum j. The solid lines correspond to $j = 0.2$, while dotted lines denote $j = 0.4$ and dashed curves denote $j = 0.6$.

and 450 Hz orbital frequency at the radius ISCO is calculated as in the following;

$$\nu_{ISCO} \approx (\frac{c^3}{2\pi 6^{3/2} GM})(1 + 0.75j) \tag{5.2}$$

Even if the lowest mass limit is taken into account, the angular momentum must be $j \geq 0.15$ in order to generate 450 Hz QPO as shown in the Figure 6.1. The Keplerian frequency is the highest frequency produced at some radius even 450 Hz may not be produced by the Keplerian motion of the matter.

Recent theoretical works show that the QPO mechanism in both neutron star systems and black hole binaries is attributed to the relativistic frequencies in the inner accretion disk (Keplerian, the periastron and nodal precession frequencies) and explained with relativistic precession models (Stella et al. 1999, Psaltis & Norman 2001). Psaltis, Belloni & van der Klis (1999) suggested that the lower kilohertz QPO produced in neutron star systems and 300 Hz QPO in GRO J1655-40 are identified QPOs. To test whether the kilohertz QPO mechanism in neutron star is associated with the twin QPOs seen in the black hole binaries,we plotted the radial frequency versus the Keplerian frequency for the mass range given in the Shahbaz et al. (1999) ($5.5M_{\odot} \leq M \leq 7.9M_{\odot}$) for different values of dimensionless angular momentum j (curved traces)(see Figure 6.2). The relativistic models denote the radial epicyclic frequency as the frequency difference between the high frequency QPOs (see chapter Review for more explanation). We also plotted the nodal precession frequency for the same mass limits and angular momenta (Strohmayer 2001).

In order to plot the radial epicyclic frequency versus Keplerian frequency we

calculated first the radial epicyclic in terms of Keplerian frequency by using the definitions below.

The radial epicyclic frequency ν_r;

$$\nu_r = \nu_\phi[1 - 6(\frac{r_g}{r}) + 8j(\frac{r_g}{r})^{3/2} - 3j^2(\frac{r_g}{r})^2]^{1/2} \tag{5.3}$$

and the orbital frequency ν_ϕ in terms of Keplerian frequency ν_K is;

$$\nu_\phi = \nu_K[1 + j(\frac{r_g}{r})^{3/2}]^{-1} \tag{5.4}$$

where

$$r_g \equiv \frac{GM}{c^2} \tag{5.5}$$

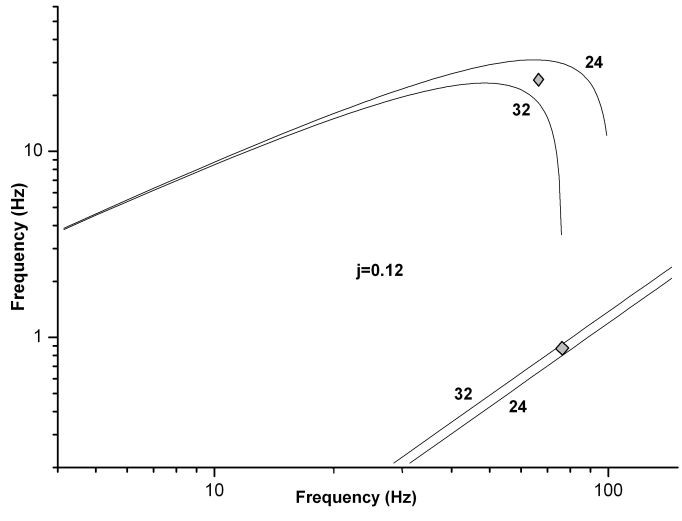

Figure 5.3: Radial epicyclic frequency (upper curves) and the nodal frequency (diagonal lines) versus Keplerian frequency for Kerr black hole with mass 24 and 32 $M_\odot$ with dimensionless angular momentum $j = 0.12$. The solid lines correspond to $j = 0.2$, while dotted lines denote $j = 0.4$ and dashed curves denote $j = 0.6$.

and $j \equiv \frac{Jc}{GM}$ is the Kerr angular-momentum parameter which is $0 < j < 1$, J is the angular momentum of the central object (van der Klis 1989).

In the Figure 6.3 we plot the the radial epicyclic frequency versus nodal frequency as a function of Keplerian frequency for a range of black hole masses with dimensionless angular momentum j. The 67 Hz and 40 Hz is plotted as diamonds in the Figure 6.3. The 67 Hz and 40 Hz QPOs can be identified with the Keplerian and radial epicyclic frequency. A ~ 0.9 Hz QPO sometimes appear with 67 Hz QPO (Morgan et al. 1997). For $j \sim 0.12$, ~ 0.9 Hz QPO may identifies the nodal precession frequency but it always is not observed at the same time with 67 Hz and 40 Hz QPOs. If this model is applicable to black hole systems, we may limit the black hole mass and angular momentum.

REFERENCES

[1] Ables, J. G., 1969,ApJ, 155L, 27A

[2] Abramowicz, M. A., & Kluzniak, W., 2001, A&A, 374, L19-L20

[3] Agrawal P. C., Paul B., Rao A. R., et al., 1996, J. Korean Astron. Soc. 29, S429

[4] Alpar, M. A., Shaham, J., 1985, Nature, 316, 239A

[5] Bailyn, C. D., Orosz, J. A., McClintock, J. E., Remillard, R. A., 1995b, Nature, 378, 157

[6] Balbus, S. A., Hawley, J. F., 1991, ApJ, 376, 214B

[7] Blandford, R. D., Konigl, A., 1979, ApJ, 232, 34B

[8] Blandford, R. D., Payne, D. G., 1982, MNRAS, 199, 883B

[9] Blandford, R. D., Znajek, R. L., 1977, MNRAS, 179, 433

[10] Brandt H. V., Rothschild, R. E., & Swank, J. H. 1993, A&AS, 97, 335

[11] Borozdin, K. N., Aleksandrovich, N. L., et al., 1997, in Matsuoka, M., Kawai N., eds, All-Sky X-ray Observations in the Next Decade, Riken, p.49

[12] Brocksopp, C., Fender, R. P., Larionov, V., Lyuty, V. M. Tarasov, A. E., Pooley, G. G., Paciesas, W. S., Roche, P., 1999, MNRAS, 30, 1063B

[13] Carpenter, G. F., Eyles, C. J., Skinner, G. K., 1977, MNRAS, 179P, 27C

[14] Castro-Tirado A.J., Brandt S., Lund N., et al., 1994, ApJS 92, 469

[15] Castro-Tirado A.J., Geballe T.R., Lund N., 1996, ApJ 461, L99

[16] Chakrabarti, S. K., Molteni, D., 1995, MNRAS, 272, 80C

[17] Chakrabarti, S. K., & Manickam, S. G., 2000, ApJ, 531, L41-L44

[18] Chapius C., Corbel S., 2004, A&A, 414, 659

[19] Chaty S., Rodrguez L. F., Mirabel I. F., Geballe T. R., Fuchs Y., Claret A., Cesarsky C. J., Cesarsky D., 2001, A&A, 366, 1035

[20] Chen X., Swank J.H., Taam R.E., 1997, ApJ 477, L41

[21] Corbel, S., Fender, R. P., Tzioumis, A. K., Nowak, M, 2000, A&A, 359, 251C

[22] Corbel, S., Kaaret, P., Jain, R.K., et al., 2001, ApJ 554, 43-48

[23] Corbel, S., Fender, R. P., 2002, ApJ, 573L, 35C

[24] Corbel, S., Nowak, M. A., Fender, R. P., 2003, A&A, 400, 1007C

[25] Crary, D. J., Kouveliotou, C., van Paradijs, J., van der Hooft, F, et al., 1996, ApJ, 463L, 79C

[26] Cui, W., Heindl, W. A., Swank, J. H., et al., 1997a, ApJ, 487, L73-L76

[27] Cui, W., Zhang, S. N., Chen, W., 1998, ApJ, 492, L53

[28] Cui, W., Zhang, S. N., Chen, W., Morgan, E. H., 1999, ApJ, 512L, 43C

[29] Cui, W., Shrader, C. R., Haswell, C. A., & Hynes, R. I., 2000a, ApJ, 535, L123-L127

[30] Das, T. K., Rao, A. R., Vadawale, S. V., 2003, MNRAS, 343, 443D

[31] Dhawan, V., Mirabel, I. F., Rodrguez, L. F., 2000, ApJ, 543, 373D

[32] Done, C.,Wardzinski, G., Gierlinski, M., 2004, MNRAS 349, 393

[33] Eikenberry, S. S., Matthews, K., Morgan, E. H., Remillard, R. A., & Nelson, R. W. 1998b, ApJ, 494, L61

[34] Eikenberry, S. S., Bandyopadhyay, R. M., 2000, ApJ, 545L, 131E

[35] Esin, A. A., McClintock, J. E., & Narayan, R., 1997, ApJ, 489, 865-889

[36] Esin, A. A., McClintock, J. E., Drake, J. J., et al., 2001, ApJ, 555, 483-488

[37] Falcke, H., Biermann, P. L., 1996, A&A, 308, 321F

[38] Falcke, H., Biermann, P. L., 1999, A&A, 342, 49F

[39] Fender, R. P., et al., 1999, MNRAS, 304, 865

[40] Fender, R., Corbel, S., Tzioumis, T., et al., 1999, ApJ, 519, L165-L168

[41] Fender, R. P., 2001, MNRAS, 322, 31F

[42] Fender, R., 2002, LNP, 589, 101F

[43] Fender, R., Maccarone M., 2003, astro-ph/0310538

[44] Fender, R. P., Gallo, E., Jonker, P. G., 2003, MNRAS, 343L, 99F

[45] Frontera, F., Zdziarski, A. A., Amati, L., et al., 2001b, ApJ, 561, 1006-1015

[46] Fuchs, Y., Rodriguez, J., Mirabel, I. F., Chaty, S., 2003, A&A, 409L, 35F

[47] Gallo, E., Fender, R. P., Pooley, G. G., 2003, MNRAS, 44, 60G

[48] Gallo, E., Fender, R. P., 2005, MmSAI, 76, 600G

[49] Garcia, M. R., McClintock, J. E., Narayan, R.,et al., 2001, ApJ, 553L, 47G

[50] Gierlinski, M., Zdziarski, A.A., Poutanen, J., et al., 1999, MNRAS, 309, 496-512

[51] Goldwurm, A., 2002, astro-ph/0212502v1

[52] Gregory, P. C., Kronberg, P. P., Seaquist, E. R., 1972, Nature, 239, 440G

[53] Greiner, J., Predehl, P., Pohl, M., 1995, A&A, 297L, 67G

[54] Greiner, J., 1996, A&AS, 120C, 239G

[55] Greiner J., Cuby J. G., McCaughrean J., 2001, Nature, 414, 522

[56] Grove, J. E., Johnson, W. N., Kroeger, R. A., et al., 1998, ApJ, 500, 899-908

[57] Gruber, D. E., Blanco, P. R., Heindl, W. A., Pelling, M. R., Rothschild, R. E., & Hink, P. L. 1996, BAAS, 120, 641

[58] Hameury, J. M., Lasota, J. P., McClintock, J. E. & Narayan, R., 1997, ApJ, 489, 234-243

[59] Hannikainen, D., Hunstead, R., Campbell-Wilson, D., 1998, NewAR, 42, 601H

[60] Hannikainen, D., Wu, K., Campbell-Wilson, D., 2001, Egru Conference, 291H

[61] Harlaftis, E. T., Greiner, J., 2004, A&A, 414L, 13H

[62] Harmon, B. A., et al., 1995, Nature, 374, 703

[63] Harmon B. A., Paciesas, W. S., & Fishman, G. J. 1992, IAU Circ., 5619

[64] Hjellming, R. M., Wade, C. M., 1971, ApJ, 170, 523W

[65] Hjellming, R. M., Wade, C. M., 1971, ApJ, 164L, 1H

[66] Hjellming, R. M., Gibson, D. M., Owen, F. N., 1975, Naturel, 256, 111H

[67] Hjellming, R. M., & Johnston, K. J., 1988, ApJ, 328, 600H

[68] Hjellming, R. M., & Johnston, K. J., 1981, ApJ, 246L, 141H

[69] Hjelming, R. M. & Rupen, M.P. 1995, Nature, 375, 464

[70] Homan, J., Mendez, M., Wijnands, R., van der Klis, M., van Paradijs, J., 1999, ApJ, 513L, 119H

[71] Homan, J., Wijnands, R., van der Klis, M., et al., 2001, ApJS, 132, 377-402

[72] Hunstead, R., Campbell-Wilson, D., 1996, IAU Circ,6410

[73] Hynes, R.I., Haswell, C. A., et al., 1998b, MNRAS, 300, 64

[74] Hynes, R. I., O'Brien, K., Horne, K., et al., 1998c, MNRAS, 299L, 37H

[75] Israelian, G., Rebolo, R., Basri, G., Casares, J., Martin, E. L, 1999, Nature, 401, 142I

[76] Jahoda, K. and McCammon, D., 1988, Nuclear Instruments and Methods in Physics Research A272, 800

[77] Kaaret, P., Corbel, S., Tomsick, J. A., 2003, ApJ, 582, 945K

[78] Kaiser, C. R., Sunyaev, R., Spruit, H. C.,2000, A&A, 356, 975K

[79] Kato, M., 1985, Nature, 316, 239A

[80] Klein, R. I., Jernigan, J. G., Arons, J., 1996, ApJ, 469L, 119K

[81] Kong, A. K. H., McClintock, J. E., Garcia, M.R. et al.,2002, ApJ, 570, 277-286

[82] Kotani, T., Ebisawa, K.,Dotani, K., et al., 2000, ApJ, 539, 413

[83] Kroeger, R. A., Strickman, M. S., Grove, J. E., et al., 1996, A&AS, 120C, 117K

[84] Kubota, A., Makishima, K., 2004, ApJ, 601, 428K

[85] Kuulkers, E., 1998, New Astronomy Reviews, 42, 1

[86] Kuulkers, E., Fender, R. P., Spencer, R. E., Davis, R. J., Morison, I., 1999, MNRAS, 306, 919

[87] Lamb, F. K., Miller, M. C., 1999, AAS, 195.0711L

[88] Laurent, P., & Titarchuk, L. 1999, ApJ, 511, 289

[89] Leahy, D. A., Darbro, W., Elsner, R. F., Weisskopf, M. C., Kahn, S., 1983, ApJ, 266, 160L

[90] Lee, J. C., Reynolds, C. S., et al., 2002, ApJ, 567, 1102-1111

[91] Levine A., Bradt H., Cui W., Jernigan J.G., Morgan E., Remillard R., Shirey R., Smith D.A., 1996, ApJ 469, L33

[92] Levinson, A.; Mattox, J. R., 1996, ApJ, 462L, 67L

[93] Liu, Q. Z., van Paradijs, J., & van den Heuvel, E. P. J., 2000, A&As, 147, 25-49

[94] Livio, M., Pringle, J. E., King, A. R., 2003, ApJ, 593, 184L

[95] Lonagir, M., 1992, High Energy Astrophysics, Cambridge University Press

[96] Lynden-Bell, D., 2003, MNRAS, 341, 1360L

[97] Markoff, S., Falcke, H., & Fender, R., 2001, A&A, 372, L25-L28

[98] Markoff, S., Nowak, M., Corbel, S.,et al., 2003, New Astronomy Reviews, 47, 491M

[99] Markovic, D. & Lamb, F. K., 1998, ApJ, 507, 316-326

[100] Markovic, D. & Lamb, F. K., 2000, HEAD, 5.2908M

[101] Mart, J., Mirabel, I. F., Rodrguez, L. F., Smith, I. A., 2002, A&A, 386,571M

[102] McClintock, J.E., Narayan, R., Garcia, M.R., et al. 2003a, ApJ, 593, 435M

[103] McClintock, J. E., Remillard, R. A., 2004, astro-ph/0306213

[104] McClintock, J. E., Horne, K., & Remillard, R. A., 1995, ApJ, 442, 358-365

[105] McClintock, J. E., Haswell, C. A., Garcia, M. R., et al., 2001b, ApJ, 555, 477-482

[106] Meier, D. L., 2002, AAS, 200, 5104M

[107] Meier, D, L., Koide, S., Uchida, Y., 2001, Science, 291, 84M

[108] Mendez, M., & van der Klis, M., 1997, ApJ, 479, 926-932

[109] Mendez, M., Belloni, T., & van der Klis, M., 1998, ApJ, 499, L187

[110] Menou, K., Esin, A. A., Narayan, R., et al., 1999, ApJ, 520, 276-291

[111] Miller, M. C., Lamb, F. K., Psaltis, D., 1998,ApJ, 508,7 91M

[112] Miller, M. C., 1999, ApJ, 520, 256M

[113] Mirabel, I. F., Rodriguez, L. F., 1994, Nature, 371, 46M

[114] Mirabel, I. F., Dhawan, V., Chaty, S., Rodriguez, L. F., Marti, J., 1998, A&A, 330L, 9M

[115] Mirabel, I. F., & Rodriguez, L. F., 1999, ARA&A, 37, 409-443

[116] Mitsuda, K., Inoue, H., Koyama, K., et al., 1984, PASJ 36, 741-759

[117] Miyamoto, S., & Kitamoto, S., 1991, ApJ, 374, 741-743

[118] Miyamoto, S., Kimura, K., Kitamoto, S., Dotani, T., 1991, ApJ, 383, 784M

[119] Miyamoto, S., Iga, S., Kitamoto, S., & Kamado, Y., 1993, ApJ, 403, L39-L42

[120] Morgan, E. H., Remillard, R. A., & Greiner, J., 1997, ApJ, 482, 993

[121] Morrison, R., & McCammon, D. 1983, ApJ, 270, 119

[122] Muno, M. P., Morgan, E. H., & Remillard, R. A. 1999, ApJ, 527, 321

[123] Muno, M. P., Morgan, E. H., Remillard, R. A., et al., 2001, ApJ, 556, 515-532

[124] Narayan, R., Quataert, E., Igumenshchev, I. V., Abramowicz, M. A., 2002, ApJ, 577, 295N

[125] Narayan, R., McClintock, J. E., & Yi, I. 1996, ApJ, 457, 821-833

[126] Narayan, R., Mahadevan, R., & Quataert, E., astro-ph/9803141

[127] Narayan, R., Garcia, M. R. & McClintock, J. E., 1997, ApJ, 478, L79-82

[128] Nobili, L., Turolla, R., Zampieri, L., & Belloni, T., 2000, ApJ, 538, L137-L140

[129] Nobili, L., 2003, ApJ, 582, 954N

[130] Nowak, M. A., 1995, PASP, 107, 1207N

[131] Nowak, M. A., Wagoner, R. V., 1993, ApJ, 418, 187N

[132] Nowak, M. A., Wagoner, R. V., Begelman, M. C., Lehr, D. E., 1997, ApJ, 477L, 91N

[133] Nowak, M. A., Lehr, D. E., 1998, in Abromowicz, M. A.,Pringle, J. E., Theory of Blackhole Accretion Disks, Cambridge Univ. Press, p.233

[134] Orosz, J. A., & Bailyn, C. D. 1997, ApJ, 477, 876

[135] Paul, B., Agrawal, P. C., Rao, A. R., et al., 1998, ApJ, 492L, 63P

[136] Phinney, E. S., 1982, MNRAS, 198, 1109P

[137] Psaltis, D., Belloni, T., & van der Klis, M., 1999, ApJ, 520, 262270

[138] Psaltis, D., & Norman, C., 2001, ApJ, astro-ph/0001391

[139] Perez, C. A., Silbergleit, A. S., Wagoner, R. V., Lehr, D. E., 1997, ApJ, 476, 589P

[140] Poutanen, J. and Fabian, A. C., 1999, MNRAS, 306, L31-L37

[141] Quataert, E., & Narayan, R., 1999, ApJ, 520, 298-315

[142] Rao, A. R., Yadav, J. S., Paul, B., 2000, ApJ, 544, 443R

[143] Rao, A. R., & Wadavale, S. V., Egru Conference, 437R

[144] Rau, A., & Greiner, J., 2003, A&A, 397, 711

[145] Rees, M. J., Phinney, E. S., Begelman, M. C., Blandford, R. D., 1982, Nature, 295, 17R

[146] Remillard, R. A., Brandt, H., Cui, W., Levine, A. M., Morgan, E. H., Shirey, B., & Smith, D. 1996, IAU Circ. 6393

[147] Remillard, R. A., Morgan, E. H., Mcclintock, J. E., Bailyn, C. D., & Orisz, J. A. 1999b, ApJ, 522, 397

[148] Remilard, R. A., Morgan, E. H., Levine, A., McClintock, J., Sobzcak, G., Bailyn, C., Jain, R., & Orosz, J., 1999a, IAU Circ., 7123, 2

[149] Remillard, R. A., & Morgan, E. H., 1999, Bull. AAS 31, 1421

[150] Remillard, R. A., 2001, astro-ph/0103431

[151] Remillard, R. A., astro-ph/0504126

[152] Remillard, R. A., Muno, M. P., McClintock, J. E. and Orosz, J. A., 2003b, BAAS, 35, 648

[153] Rodriguez, L. F., Mirabel, I. F., Marti, J., 1992, ApJ, 401L, 15R

[154] Silbergleit, A. S., Wagoner, R. V., Ortega-Rodrguez, M., 2001, ApJ, 548, 335S

[155] Shahbaz, T., van der Hooft, F., Casares, J., Charles, P. A., & van Paradijs, J. 1999, MNRAS, 306, 89

[156] Shakura, N. I., & Sunyaev, R. A., 1973, A&A, 24, 337-366

[157] Sobzcak, G. J., McClintock, J. E., et al., 1999, ApJ, 520, 776

[158] Sobczak, G. J., McClintock, J. E., Remillard, R. A., et al., 2000a, ApJ, 531, 537-545

[159] Spencer, R. E., 1979, Nature, 282, 483S

[160] Stella, L., Vietri, M., 1998, ApJ, 492L, 59S

[161] Stella, L., Vietri, M., & Morsink, S.M., 1999, ApJ 524, L63-L66

[162] Stirling, A. M., Spencer, R. E., de la Force, C. J., et al., 2001, MNRAS, 327, 1273S

[163] Strohmayer, T. E., Zhang, W., Swank, J. H., 1996, ApJ, 469L, 9S

[164] Strohmayer, T., 2001, ApJ, 552, L49, L53

[165] Strohmayer, T., 2001b, ApJ, 554, L169, L172

[166] Tagger, M. & Pellat, R., 1999, A&A, 349, 1003-1016

[167] Tananbaum, H., Gursky, H., Kellogg, E., et al., 1972, ApJ, 177, L5-L10

[168] Tigelaar, S. P., Fender, R. P., Tilanus, R. P. J., Gallo, E.,Pooley, G., 2004, MNRAS, 352, 1015T

[169] Tingay, S. J., et al., 1995, Nature, 374, 141

[170] Titarchuk, L., & Osherovich, V., 2000, ApJ, 542, L111-L114

[171] Tomsick, J. A., Kaaret, P., Kroeger, R.A. and Remillard, R.A., 1999b, ApJ, 512, 892-900

[172] Tomsick J. A., & Kaaret, P., 2001, ApJ, 548, 401-409

[173] Trudolyubov, S., Churazov, E., Gilfanov, M., et al., 1999, A&A 342, 496-501

[174] Turler, M., Courvoisier, T. J. L., Chaty, S., Fuchs, Y., 2004, A&A, 415L, 35T

[175] Turner, N. J., Stone, J. M., Sano, T., 2002, ApJ, 566, 148T

[176] Ueda, Y., Inoue, H., Tanaka, Y., Ebisawa, K., 1998, ApJ, 500, 1069U

[177] Vadawale, S. V., Rao, A. R., Naik, S., et al., 2003, ApJ, 597, 1023V

[178] van der Hooft, F., Heemskerk, M. H. M., Alberts, F., van Paradijs, J., 1998, A&A, 329, 538V

[179] van der Klis, M., 1989, ARA&A, 27, 517V

[180] van der Klis, M. , 1995, in Xray Binaries, eds. Lewin W.H.G.,van Paradijs J. & van den Heuvel E.P.J., Cambridge U. Press, Cambridge

[181] van der Klis, M., Swank, J. H., Zhang, W., 1996, ApJ, 469L, 1V

[182] van der Klis, M., 2000, ARA&A, 38, 717V

[183] van Paradijs, J., 1983, Adsx Conference, 192V

[184] Varniere, P., Tagger, M., 2002, A&A, 394, 329V

[185] Wade C. M., Hjellming R. M., 1971, ApJ, 170, 523W

[186] Wagoner, R. V., Silbergleit, A. S. and Ortega-Rodriguez, M., 2001, ApJ, 559, L25L28

[187] Webster, B.L and Murdin, P., 1972, Nature, 235, 37-38

[188] Zhang, S. N., et al., 1994, IAU Circ. 6046

[189] Zhang, S. N., Cui, W., & Chen, W., 1997, ApJ, 482, L155

[190] Zdziarski, A. A., 2000, astro-ph/0001078

[191] Zdziarski, A. A., Grove, J. E., Poutanen, J., Rao, A. R., & Vadawale, S. V., 2001, ApJ, 554, L45

[192] Zdziarski, A. A., 2005, astro-ph/0504018